

Supporting information for:

Regionalized life cycle inventories of global sulfidic copper tailings

Lugas Raka Adrianto*, Stephan Pfister, Stefanie Hellweg

Chair of Ecological Systems Design, Institute of Environmental Engineering, ETH Zurich, John-von-Neumann-Weg 9, Switzerland

*Email: adrianto@ifu.baug.ethz.ch

Supporting Information-1 (SI-1)

63 Pages

30 Figures

18 Tables

**Data analysis and visualization in this manuscript are made possible with R (v 4.0)¹ + libraries (ggplot², ggpurr, dplyr), Tableau (v2020.3)³, and Microsoft Excel 365 software (v2019)⁴*

Table of Contents

List of Figures	3
List of Tables.....	6
S1. Copper sites coverage in this study	8
S2. Classification of copper production process	9
S3. Mineral process modelling in HSC Sim©.....	11
S4. Additional details for copper compositions.....	15
S5. Further descriptions of PHREEQC modelling and input parameters.....	17
S6. Net infiltration map (groundwater recharge) using GLOBWB model.....	28
S7. Baseline scenario: Environmental hotspots.....	29
S8. Primary copper production data for 2019 – 2050.....	31
S9. Freshwater ecotoxicity impacts from baseline year 2019 to 2050	33
S10. Compare tailings characteristics from model prediction vs. tailings characteristics from actual data.....	34
S11. Aggregated results for long term horizon.....	37
S12. Impacts of climate conditions and ore deposit types (complementary results).....	40
S13. Compiled copper production data for 2019.....	44
S14. Freshwater ecotoxicity results across continents and countries	45
S15. Complementary LCA results: 1) USEtox human toxicity, midpoint, 2) ReCipe, endpoint single score, 3) EF 3.0, endpoint single score	48
S16. Further discussions and limitations on main waste streams in mining, rehabilitation, and tailings management.....	50
S17. By-products and allocation in metal mining systems.....	54
S18. Further supporting information	57

References	58
------------------	----

List of Figures

Figure S1. A simplified Outotec© HSC Sim 10 flowsheet for copper beneficiation process with ore deposit as input. Red dashed box indicates the main flotation controls in the simulation.....	11
Figure S2. An example of flotation unit module in HSC Chemistry 10. Parameterizations are performed by accessing model tabs on the left.	12
Figure S3. Method for estimating the tailings composition from different ore deposit types	12
Figure S4. Mineral to Element Conversion in HSC Sim 10	15
Figure S5. The changes of composition for porphyry copper deposits feed when the grades vary (an example for illustrative purposes)	16
Figure S6. Porphyry tailings: Modeled leachate concentrations of As, Cd, Cu, Pb and Zn, according to the geochemical model up to 150k years after disposal of porphyry tailings. EU groundwater leachate discharge threshold values ⁴⁷ are displayed for comparison	24
Figure S7. Volcanogenic massive sulfide tailings: Modeled leachate concentrations of As, Cd, Cu, Pb and Zn, according to the geochemical up to 150k years after disposal of volcanicogenic massive sulfide tailings. EU groundwater leachate discharge threshold values ⁴⁷ are displayed for comparison	24
Figure S8. Skarn tailings: Modeled leachate concentrations of As, Cd, Cu, Pb and Zn, according to the geochemical up to 150k years after disposal of skarn tailings. EU groundwater leachate discharge threshold values ⁴⁷ are displayed for comparison	25
Figure S9. Sediment hosted tailings: Modeled leachate concentrations of As, Cd, Cu, Pb and Zn, according to the geochemical up to 150k years after disposal of sediment hosted tailings. EU groundwater leachate discharge threshold values ⁴⁷ are displayed for comparison	25

Figure S10. Magmatic sulfide tailings: Modeled leachate concentrations of As, Cd, Cu, Pb and Zn, according to the geochemical up to 150k years after disposal of magmatic sulfide tailings. EU groundwater leachate discharge threshold values ⁴⁷ are displayed for comparison	26
Figure S11. Iron oxide tailings: Modeled leachate concentrations of As, Cd, Cu, Pb and Zn, according to the geochemical up to 150k years after disposal of iron oxide tailings. EU groundwater leachate discharge threshold values ⁴⁷ are displayed for comparison	26
Figure S12. Intrusion-related tailings: Modeled leachate concentrations of As, Cd, Cu, Pb and Zn, according to the geochemical up to 150k years after disposal of intrusion-related tailings. EU groundwater leachate discharge threshold values ⁴⁷ are displayed for comparison	27
Figure S13. Epithermal tailings: Modeled leachate concentrations of As, Cd, Cu, Pb and Zn, according to the geochemical up to 150k years after disposal of epithermal tailings. EU groundwater leachate discharge threshold values ⁴⁷ are displayed for comparison	27
Figure S14. Top: The conceptual water flows in PCR-GLOBWB, redrawn from Sutanudjaja et al. ⁴⁸ . Bottom: The annual groundwater recharge, taken from the results of PCR-GLOBWB in mm per year ^{48,49} . Abbreviations: PREC= Precipitation, E= Evaporation, P= Percolation/ capillary rise, QDR= Direct run-off, QSF= Interflow or subsurface stormflow, QBF= Baseflow, QChannel= Discharge along the channel.....	28
Figure S15. LCA system boundary to produce 1 kg copper	29
Figure S16. The procedure to systematically compare generated tailings inventory data (this study) with the available ones in LCA database	30
Figure S17. Future copper supply estimation and data compilation	31
Figure S18. The cases for preproduction sites with three different categories of greenfield mining. Adapted after ICMM ⁵³	32

Figure S19. Comparison of metal compositions from simulated results vs. collected data from mining partners. The upper limit of the whisker represents worst case with worse flotation performance, and the lower limit represents better flotation performance.	34
Figure S20. Comparison of metal compositions from simulated results x-axis vs. tailings data from Chilean sites y-axis. Blue circles represent results from base calculation, while green triangles are averaged sampling data from survey. Whiskers represent the highest and lowest value in the dataset (vertical) and simulated results (horizontal), respectively.....	35
Figure S21. Contribution to global ecotoxicity impacts in 2019 per continent and country, illustrated in tree map chart. The area of each region and country is proportional to the estimated emissions.	39
Figure S22. Distribution of ecotoxicity, grouped by net infiltration. The x-axis (copper deposit type) is ordered, based on the overall median of each class.....	40
Figure S23. Histogram, shared x-axis (toxicity), grouped by deposit types. Dashed lines indicate median.	41
Figure S24. Regression Line, Cu grade vs. Toxicity per deposit type (left) and overall (right)....	41
Figure S25. Scatter plots with regression lines: Net infiltration vs. Toxicity	42
Figure S26. LCA of copper production (method: USEtox)—a) short-term and b) long-term in different regions. Data to generate this chart is available in Table S3.....	46
Figure S27. Freshwater ecotoxicity per ton of tailings in log-scale for short-term and long-term horizons	47
Figure S28. LCA results of 1 kg copper production. (A) ReCiPe single score, endpoint, incl. long-term emissions and (B) EF single score, endpoint, incl. long-term emissions)	49
Figure S29. Simplified mining process flowsheets with the source of main waste flows (adapted from Lebre et al. ⁷⁰)	51

Figure S30. A cross-section of typical volcanogenic massive sulfide (VMS) as seen in the sedimentary record⁸⁶, image adapted from VMS webpage⁸⁷ 55

List of Tables

Table S1. Global copper deposits coverage in terms of production, ore tonnage, and grades around the world.....	8
Table S2. Flotation kinetic parameters and data sources used in the beneficiation modelling	13
Table S3. Generic chemical compositions taken from HSC Geo Database.....	14
Table S4. Parameters used in PHREEQC simulations.....	18
Table S5. Initial composition of tailings from porphyry deposit	18
Table S6. Initial composition of tailings from volcanogenic massive sulfide deposit.....	19
Table S7. Initial composition of tailings from skarn deposit	19
Table S8. Initial composition of tailings from sediment hosted deposit	20
Table S9. Initial composition of tailings from magmatic sulfide deposit	20
Table S10. Initial composition of tailings from iron oxide deposit.....	21
Table S11. Initial composition of tailings from intrusion related deposit.....	21
Table S12. Initial composition of tailings from epithermal deposit.....	22
Table S13. Geochemical thermodynamic reactions included in the simulation from PHREEQC database ³⁷ and WATEQ4F database ³⁰	23
Table S14. Summary of results for the ecotoxicity projection from 2019 to 2050 in all countries (Unit: CTUe per year, method: USETox)	33
Table S15. Comparison of approximated results for three flotation cases vs. plant data	34
Table S16. The summary of aggregated freshwater ecotoxicity (long-term horizon) results in this study. The data is also derived from previous figures.....	37

Table S17. Copper production from sulfides in 2019, compiled (only listed as an illustration in this document. For complete list, see Supporting Information-2).....	44
Table S18. Comparison of ecotoxicity (method: USEtox) results: Our study vs. Ecoinvent 3.6, aggregated following regions in the copper datasets.....	45

S1. Copper sites coverage in this study

Table S1. Global copper deposits coverage in terms of production, ore tonnage, and grades around the world

Ore deposit type	Production in Mt	Cumulative Production (% total of this study)	Nr. of sites	Ranges of Tonnage (median) in Mt	Ranges of Cu- grades (median) in %w	Important countries or regions
Porphyry	11.8	61%	202	0.6 – 21,277 (288)	0.1 – 1.5 (0.6)	China, North America, Latin America
Sediment-hosted Stratiform/ Strata bound Cu	3.9	20%	45	0.9 – 3,230 (72)	0.46 – 4.38 (1.3)	USA, Poland, Central Africa
Volcanogenic massive sulfide (VMS)	1.6	8%	65	1 – 334 (23)	0.19 – 4.7 (1)	Canada, Australia, Europe
Skarn	1.1	6%	29	0.4 – 10,060 (72)	0.07 – 2.19 (1.3)	China, Latin America
Iron-oxide Cu-Au (IOCG)	0.5	3%	15	3.2 – 329 (100)	0.07 – 3.09 (0.7)	Australia, Latin America
Magmatic sulfide	0.4	2%	52	1.8 – 3,709 (36)	0.01 – 1.82 (0.4)	China, USA, Central Africa
Epithermal	0.1	1%	20	0.3 – 130 (18)	0.3 – 1.83 (0.7)	Latin America, Asia
Intrusion-related Au	0.02	0.1%	1	152	0.1%	Australia
Orogenic Au	0.02	0.1%	2	2.9 – 63 (33)	0.8 – 0.9 (0.9)	Australia, China
Total copper production collected in this study (2019)	15.1	75% coverage in 2019	431			
Annual global copper production based on SNL Market Intelligence 2019 data⁵	20.5					

Note: A complete table to derive this summary is provided in Table S17 and Supporting Information-2 (S2.1). It comprises a list of 431 project IDs.

S2. Classification of copper production process

Based on the worldwide copper production practice and its classification⁶, copper production can involve a variety of approaches. Generally, it can be divided into pyrometallurgical and hydrometallurgical routes^{7,8}, as described in the following:

- **Pyrometallurgical route (the focus of this study)**

Mining-Flotation-Smelting-Refining – an open pit or underground mine extracts Cu ore (with a grade of 0.4-2% Cu), which is then processed in a flotation plant to produce a Cu-rich concentrate (typically 20-25% Cu) which is then smelted to produce Cu anode (say 95-98% Cu), in turn processed in a refinery to produce high purity Cu (>99.9% Cu).

- Examples: Australia, Canada, USA, Chile, etc.
- Around 80% of global mined Cu is produced using this technology

- **Hydrometallurgical route**

Mining-Heap Leaching-Refining – an open pit mine extracts Cu ore (the grade of 0.4-1% Cu) which is piled in large heaps, sulfuric acid is irrigated across this heap and the solution percolates through it and is captured at the bottom rich in Cu, where it is pumped to a refinery to produce high purity refined Cu.

- Examples: USA, Chile, etc.
- About 20% of global mined Cu is produced this way
- Heap leach projects are mostly based on oxide ores

Mining-Acid Leaching-Refining – an open pit or underground mine extracts Cu ore (with the grade of 1-4%Cu), which is then processed in a plant using acid to directly dissolve the Cu together with the other metals, and the solutions refined to produce high purity Cu.

- Examples: Zambia, Laos, Democratic Republic of the Congo (DRC), etc.
- About 1-2% of global mined Cu is produced this way

S3. Mineral process modelling in HSC Sim©

HSC Simulation v10⁹ for nine types of deposit, with simplified flowchart being drawn (Figure S1 and Figure S2). We used similar models as done by Michaux and Reuter's three-model component^{10,11}. The flotation parameters and recovery data from handbook^{12–14} are then supplied to the simulator to obtain results for each deposit type. Table S2 summarizes the simulation parameters, recovery efficiency, deposit types, and further assumptions in this study.

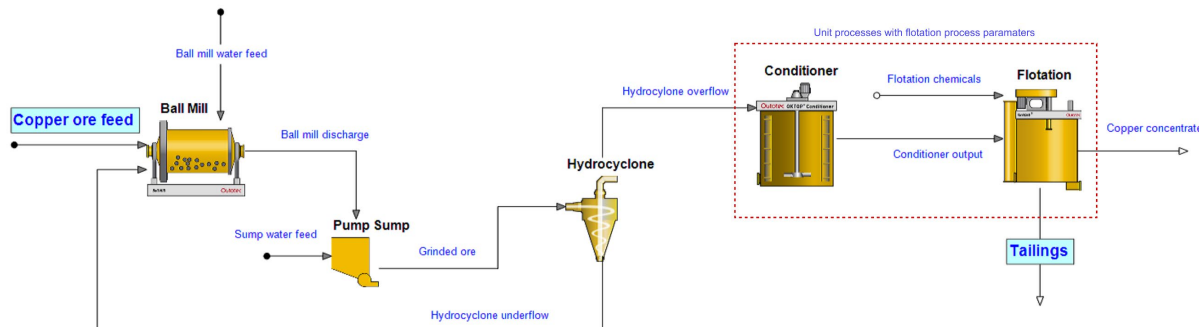


Figure S1. A simplified Outotec© HSC Sim 10 flowsheet for copper beneficiation process with ore deposit as input. Red dashed box indicates the main flotation controls in the simulation.

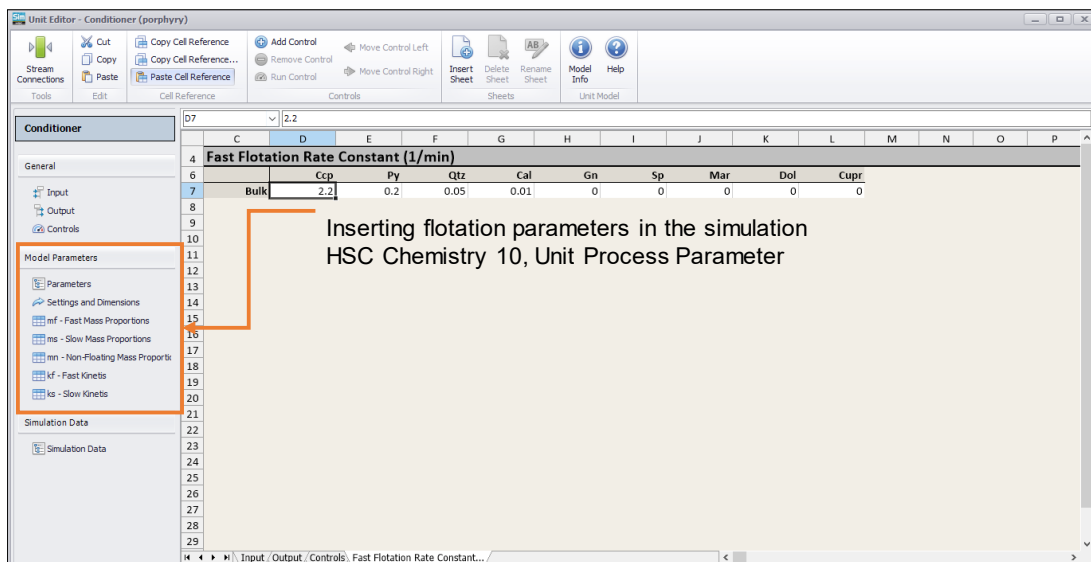


Figure S2. An example of flotation unit module in HSC Chemistry 10. Parameterizations are performed by accessing model tabs on the left.

Figure S3 presents how the tailings properties for specific ore deposits and the calculation is applicable generally.

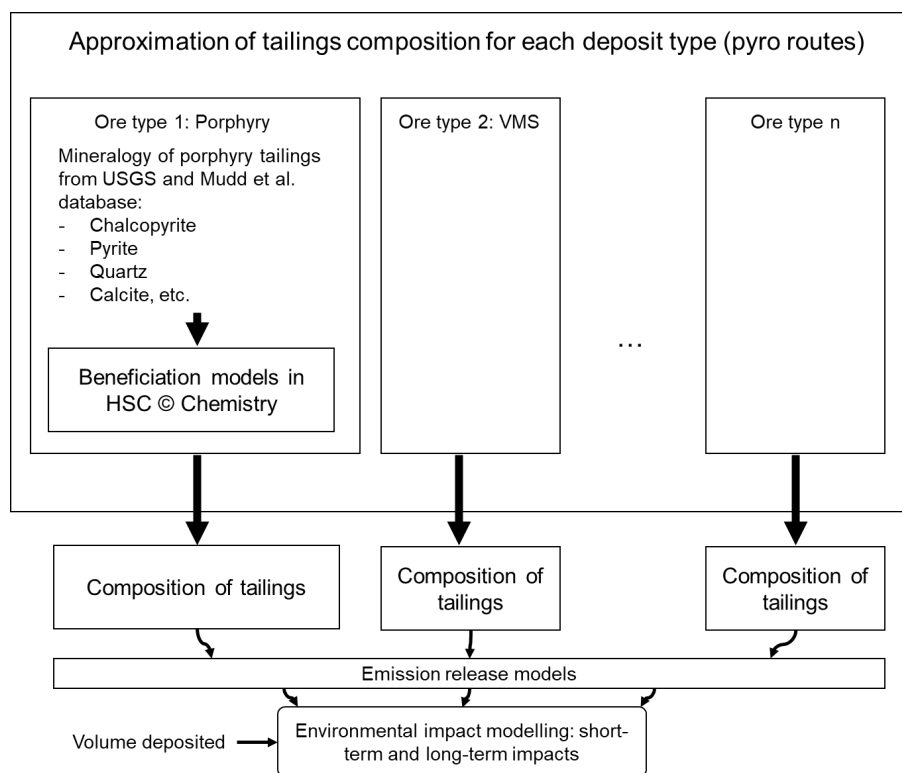


Figure S3. Method for estimating the tailings composition from different ore deposit types

Table S2. Flotation kinetic parameters and data sources used in the beneficiation modelling

Copper deposit type		Porphyry	Sediment-hosted Stratiform/ Strata bound Cu	Volcanogenic massive sulfide (VMS)	Skarn	Iron-oxide Cu-Au (IOCG)	Magmatic sulfide	Epithermal	Intrusion-related Au and orogenic Au
Sulfide minerals	Chalcopyrite (Ccp)	Chalcopyrite (Ccp)	Chalcopyrite (Ccp)	Chalcopyrite (Ccp)	Chalcopyrite (Ccp)	Cuprite (Cupr)	Chalcopyrite (Ccp)	Chalcopyrite (Ccp)	Chalcopyrite (Ccp)
	Pyrite (Py)	Pyrite (Py), Galena (Gn), Sphalerite (Sp), Marcasite (Mar)	Pyrite (Py), Galena (Gn), Sphalerite (Sp)	Pyrite (Py)	-	-	Pyrite (Py), Galena (Gn), Sphalerite (Sp)	Pyrite (Py), Galena (Gn), Sphalerite (Sp)	Pyrite (Py)
Other gangue minerals	Quartz (Qtz), calcite (Cal)	Quartz (Qtz), calcite (Cal)	Quartz (Qtz), calcite (Cal)	Quartz (Qtz), calcite (Cal)	Quartz (Qtz), dolomite (Dol)	Quartz (Qtz), calcite (Cal)	Quartz (Qtz), calcite (Cal)	Quartz (Qtz), calcite (Cal)	Quartz (Qtz), calcite (Cal)
m_f	<i>Ccp</i>	9.10E-01	1.62E+00	1.71E+00	1.55E+00	-	1.80E+00	1.26E+00	1.09E+00
	<i>Py</i>	1.00E-01	1.36E-01	1.44E-01	1.28E-01	-	8.80E-02	8.00E-02	1.10E-01
	<i>Qtz</i>	6.00E-02	6.50E-02	9.50E-02	8.40E-02	7.20E-02	7.50E-02	1.00E-01	7.20E-02
	<i>Cal</i>	2.00E-02	4.50E-02	5.40E-02	3.80E-02	-	4.80E-02	4.50E-02	2.80E-02
	<i>Gn</i>	-	2.80E-02	3.80E-02	-	-	3.20E-02	3.40E-02	-
	<i>Sp</i>	-	1.18E+00	1.82E+00	-	-	1.46E+00	1.37E+00	-
	<i>Mar</i>	-	1.12E-01	-	-	-	-	-	-
	<i>Cupr</i>	-	-	-	-	1.28E+00	-	-	-
	<i>Dol</i>	-	-	-	-	2.00E-02	-	-	-
m_s	<i>Ccp</i>	4.00E-02	1.12E-01	1.52E-01	6.40E-02	-	1.20E-01	1.52E-01	6.00E-02
	<i>Py</i>	1.50E-02	2.40E-02	3.15E-02	1.65E-02	-	1.95E-02	2.55E-02	1.65E-02
	<i>Qtz</i>	1.00E-02	1.12E-02	1.68E-02	1.40E-02	1.10E-02	1.44E-02	8.00E-03	1.10E-02
	<i>Cal</i>	-	6.40E-03	7.60E-03	1.20E-02	0.00E+00	4.40E-03	5.20E-03	-
	<i>Gn</i>	-	9.00E-03	9.50E-03	-	-	6.50E-03	8.00E-03	-
	<i>Sp</i>	-	7.60E-02	8.40E-02	-	-	7.20E-02	6.40E-02	-
	<i>Mar</i>	8.00E-03	1.80E-02	-	-	-	-	-	9.60E-03
	<i>Cupr</i>	-	-	-	-	6.00E-02	-	-	-
	<i>Dol</i>	-	-	-	-	9.60E-03	-	-	-
k_f	<i>Ccp</i>	2.20E+00	3.84E+00	6.08E+00	3.30E+00	-	5.76E+00	4.16E+00	3.30E+00
	<i>Py</i>	2.00E-01	1.20E-01	2.10E-01	3.20E-01	-	1.90E-01	1.30E-01	3.00E-01
	<i>Qtz</i>	5.00E-02	5.60E-02	7.20E-02	9.00E-02	6.00E-02	5.60E-02	6.00E-02	5.00E-02
	<i>Cal</i>	1.00E-02	1.52E-02	1.60E-02	1.20E-02	-	1.60E-02	1.60E-02	1.20E-02
	<i>Gn</i>	-	9.50E-03	9.50E-03	-	0.00E+00	6.50E-03	8.00E-03	-
	<i>Sp</i>	-	4.62E+00	6.60E+00	-	0.00E+00	5.60E-03	6.30E-03	-
	<i>Mar</i>	-	1.40E-01	-	-	0.00E+00	0.00E+00	0.00E+00	-
	<i>Cupr</i>	-	-	-	-	4.32E+00	-	-	-
	<i>Dol</i>	-	-	-	-	1.20E-02	-	-	-
k_s	<i>Ccp</i>	2.00E-02	1.10E-02	1.80E-02	3.80E-02	-	1.20E-02	2.00E-02	2.60E-02
	<i>Py</i>	1.00E-02	6.50E-03	1.00E-02	1.50E-02	1.50E-02	6.00E-03	1.00E-02	1.40E-02
	<i>Qtz</i>	1.00E-03	6.00E-04	1.00E-03	1.80E-03	-	6.00E-04	6.00E-04	1.30E-03
	<i>Cal</i>	1.00E-02	5.40E-03	6.00E-03	1.90E-02	-	3.60E-03	5.70E-03	1.50E-02
	<i>Gn</i>	-	1.60E-04	2.00E-04	-	-	1.50E-04	1.90E-04	-
	<i>Sp</i>	-	2.40E-02	3.80E-02	-	-	4.00E-02	2.20E-02	-
	<i>Mar</i>	-	7.50E-04	-	-	-	-	-	-
	<i>Cupr</i>	-	-	-	-	3.20E-02	-	-	-

Flotation kinetics parameters (m_n is calculated via mass balance)

	Dol	-	-	-	1.50E-03	-	-	-
Reagents/ ancillaries	Cu recovery ranges from 80 - 92%; Xanthate as the main collector with basic pH conditions	Cu recovery ranges from 78-87%; Reagents for bulk process: CaO 700 g/t, Na ₂ SO ₃ 800 g/t	Cu recovery ranges from 81-95%; Reagents for bulk process: Na ₂ S ₂ O ₈ 2000 g/t, CaO (pH 7.5), HQS 800 g/t	Cu recovery ranges from 80 - 92%; Behaved similar to porphyry and thus modelled as is, as inferred from the literatures	Cu recovery ranges from 75-84%; Xanthate as the main collectors. Used sulfidizers Na ₂ SiO ₃ = 300 g/t to treat dolomitic ores	Cu recovery ranges from 85-95%; Reagents: Ca(OH) ₂ 600 g/t, Na ₂ SO ₃ 500 g/t	Cu recovery ranges from 82-90%; Reagents: Ca(OH) ₂ = pH 9.5, NaCN = 300 g/t	Cu recovery ranges from 88-95%; Reagents: Na ₂ S 30 g/t
<i>Main reference "Handbook of Flotation Reagents"¹², Mineral Processing Technology¹³ and additional remarks</i>	1) Handbook of Flotation Reagents chapter 12, 2) Environmental Attributes and Resource Potential of Mill Tailings from Diverse Mineral Deposit Types ¹⁵	1) Handbook of Flotation Reagents chapter 15, 2) Other plants data and literatures ¹⁶⁻¹⁸	1) Handbook of Flotation Reagents chapter 14	1) Handbook of Flotation Reagents chapter 12, 2) Other literatures ^{19,20}	1) Handbook of Flotation Reagents chapter 19, 2) Other resource ²¹	1) Handbook of Flotation Reagents chapter 13, 2) Other literatures ^{15,22,23}	1) Handbook of Flotation Reagents chapter 13, 2) Other literatures ^{24,25}	1) Handbook of Flotation Reagents chapter 17, 2) Environmental Attributes and Resource Potential of Mill Tailings from Diverse Mineral Deposit Types ^{15, 3) Other sources^{21,26}}

Table S3. Generic chemical compositions taken from HSC Geo Database

Element	Chalcopyrite	Pyrite	Quartz	Calcite	Galena	Sphalerite	Marcasite	Cuprite
Cu	34.63							88.82
Fe	30.43	46.55					46.55	
S	34.94	53.45			13.4	32.91	53.45	
O			53.26	47.96				11.18
Si			46.74					
C				12				
Ca				40.04				
Pb					86.6			
Zn						67.09		
Mg								

S4. Additional details for copper compositions

The following examples are the procedures of how the generic composition of porphyry deposits are adjusted to the copper grade. The HSC Sim Element to Mineral Conversion “Geomodule” is used to convert the composition of ore deposit input mineralogy to achieve the target grade (in the example below, Cu-grade of 0.5%).

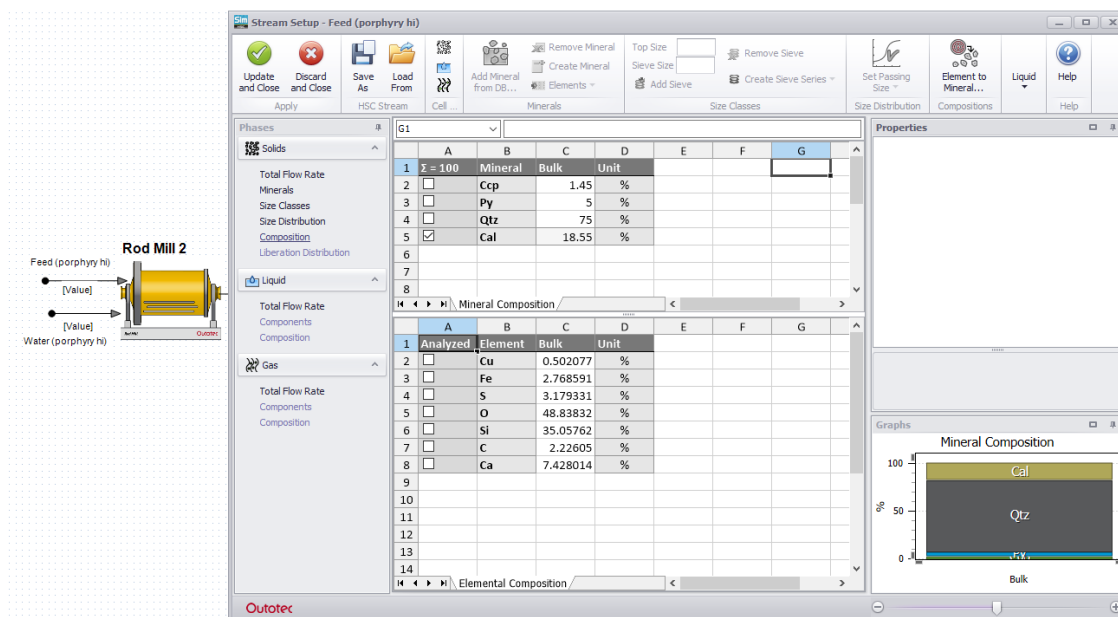


Figure S4. Mineral to Element Conversion in HSC Sim 10

The buffering capacity (i.e., calcite) and other inert mineral (i.e., quartz) are used to equalize the compositions when copper grade increases or decreases (Figure S5). These are reflected in the output tailings after running the flotation processes of the circuit. Based on information from Heinrich and Candela (2013)²⁷, the growth of ore zone at the center determines the amounts of quartz and pyritic minerals (in this case pyrite and chalcopyrite). It implies that the more copper we have at the core in the sulfidic regions, the larger the composition of quartz, pyrite, and chalcopyrite. This is also in line with the cross-section picture of the deposit, showing that the propylitic layer that contains calcite and other minerals are only present in

the outer layer of copper deposit according to the preliminary model of copper deposits by USGS²⁸. Hence, we assumed that whenever copper grade increases, the buffering minerals will decrease.

Cu grade = 0.5%	
Mineral	Content
%w	mol/kg
Calcite	18.06
Chalcopyrite	1.45
Pyrite	5.07
Quartz	75.00
Ca(OH)2	0.3000
Cd(OH)2	0.0121
Zn(OH)2	0.0967
Pb(OH)2	0.0011
Cu(OH)2	0.0126
As, on OH sites	0.0026
Secondary minerals	
CdCO3	Secondary mineral
ZnCO3	Secondary mineral
CuCO3	Secondary mineral
PbCO3	Secondary mineral
CdO	Secondary mineral
PbO	Secondary mineral
ZnO	Secondary mineral
Cu2O	Secondary mineral

Cu grade = 0.1%	
Mineral	Content
%w	mol/kg
Calcite	25.23
Chalcopyrite	0.29
Pyrite	4.77
Quartz	69.4
Ca(OH)2	0.3000
Cd(OH)2	0.0003
Zn(OH)2	0.0027
Pb(OH)2	0.0002
Cu(OH)2	0.0025
As, on OH sites	0.0026
Secondary minerals	
CdCO3	Secondary mineral
ZnCO3	Secondary mineral
CuCO3	Secondary mineral
PbCO3	Secondary mineral
CdO	Secondary mineral
PbO	Secondary mineral
ZnO	Secondary mineral
Cu2O	Secondary mineral

Cu grade = 1%	
Mineral	Content
%w	mol/kg
Calcite	8.60
Chalcopyrite	2.90
Pyrite	5.34
Quartz	82.8
Ca(OH)2	0.3000
Cd(OH)2	0.0037
Zn(OH)2	0.0293
Pb(OH)2	0.0023
Cu(OH)2	0.0252
As, on OH sites	0.0026
Secondary minerals	
CdCO3	Secondary mineral
ZnCO3	Secondary mineral
CuCO3	Secondary mineral
PbCO3	Secondary mineral
CdO	Secondary mineral
PbO	Secondary mineral
ZnO	Secondary mineral
Cu2O	Secondary mineral

Figure S5. The changes of composition for porphyry copper deposits feed when the grades vary (an example for illustrative purposes)

We applied the procedures to other deposit types with similar characteristics with the grouping from Table S1. For porphyry copper deposits, they are assumed to contain similar mineralogy as skarn²⁰, iron oxide²¹, intrusion related Au²¹ deposits. These are simplifications to include the major primary minerals that are often present in various deposit types and are reflected in the flotation handbook by Bulatovic (2007)¹². There, volcanogenic massive sulfide, sediment-hosted, magmatic sulfide and epithermal may contain additional minerals that might affect the overall beneficiation schemes and flotation mechanisms due to the presence of galena (Pb-containing), sphalerite (Zn-containing), and marcasite (sources of FeS) in the ore growth zone. We repeated the similar procedures to the other deposits as shown in Figure S5, Figure S5, and HSC Mineral to Element Conversion in “Geomodule” by also adding the presence of the previously mentioned minerals.

S5. Further descriptions of PHREEQC modelling and input parameters

We used the coupled transport and reaction model PHREEQC and WATEQ4F^{29,30} to model heavy metal emissions from tailings deposits as a function of time. The parameters for the models are tabulated in Table S4, whereas the chemical equations are listed in Table S13. The model predicts the emissions of metals over time, following the development of pH and mineralogy changes as the solid fractions interact with the infiltrating water and simulating simple percolation scenarios. In order to do this, 1 kg of initial mineral assemblages containing a number of solubilities controlling minerals were defined. A single-cell column containing the mineral assemblage was set-up and water equilibrated with atmospheric CO₂ was shifted through the column to simulate percolation. For simplicity, only 1-D transport of eluent/ forward flow was used, while neither dispersivity nor dual-porosity were considered. Detailed explanations about this approach can be found in other prediction-based and long-term leaching studies³¹⁻³⁴.

Minerals such as calcite control the rate of heavy metal leaching due to its buffering mechanism. Thus, majority of metal emissions in this study was limited by mineral dissolution and precipitation processes. However, arsenic was modelled differently following the double-layer complexation and strong sorption on iron oxide surfaces as prescribed by Dzombak and Morel³⁵ and Appelo et al.³⁶. Activity coefficients were adjusted for an ionic strength calculated from the component's concentrations according to Debye-Hueckel³⁷. The initial mineralogical compositions or assemblages of the tailings are shown in Table S5-Table S12. We compiled a set of relevant reactions (e.g., mineral dissolution/ precipitation and surface complexation) from the main PHREEQC database, complemented with the other geochemical database such as WATEQ4F and Dzombak-Morel layer model. It was not intended to model the complete mineral composition but to include some major species

relevant for heavy metal solubility. The base sealing and the drainage system of the storage facilities are generally estimated to endure less than 100 years³⁸. Therefore, the technical barrier is only relevant for short-term emissions and will not prevent a large fraction of long-term emissions from entering the subsoil and the groundwater compartment. Hence, the technical barrier system was neglected in the present analysis.

Table S4. Parameters used in PHREEQC simulations

Parameter	Value	Unit
Infiltration rate	Annual groundwater recharge from PCR-GLOBWB (see section 3.5)	1/m ² *a
Partial pressure of CO ₂	10 ^{-3.5}	atm
Time step	1	year
Porosity	Ranges of values between 40 – 55 based on literatures ^{39–42} . 50 is chosen for the simulations	%
Tailings thickness (<i>d</i>)	20 – average: sources of data ^{43,44}	m
Tailings density (<i>ρ</i>)	2200 – average: primary industry's ⁴⁵ data and literature sources ^{40,46}	kg/m ³
Solution pH	5	
Temperature	25 – median for stored tailings: partner's data ⁴⁵	

Table S5. Initial composition of tailings from porphyry deposit

Mineral	Content	
	Wt %	(mole/kg)
Calcite	1.60E+01	1.60E+00
Chalcopyrite	1.56E-01	2.86E-02
Pyrite	5.07E+00	6.07E-01
Quartz	7.85E+01	4.71E+00
Ca(OH)2	3.00E-01	2.22E-02
Cd(OH)2	1.30E-03	1.90E-04
Zn(OH)2	1.04E-02	1.04E-03
Pb(OH)2	1.13E-04	2.73E-05
Cu(OH)2	1.36E-03	1.32E-04
As, on hydroxide sites	2.58E-03	3.45E-05
CdCO ₃ , ZnCO ₃ , CuCO ₃ , PbCO ₃ , CdO, PbO, ZnO, Cu ₂ O	secondary mineral	
Compositions taken from HSC Sim tails output		

Table S6. Initial composition of tailings from volcanogenic massive sulfide deposit

Mineral	Content	
	Wt %	(mole/kg)
Calcite	6.19E+00	6.19E-01
Chalcopyrite	4.28E-01	7.85E-02
Galena	5.57E+00	1.34E+00
Pyrite	1.05E+01	1.26E+00
Quartz	7.66E+01	4.60E+00
Sphalerite	4.00E-01	3.88E-02
Ca(OH) ₂	2.50E-01	1.85E-02
Cd(OH) ₂	7.44E-05	1.09E-05
Zn(OH) ₂	8.67E-03	8.67E-04
Pb(OH) ₂	1.64E-03	3.95E-04
Cu(OH) ₂	3.72E-03	3.63E-04
As, on hydroxide sites	3.24E-03	4.32E-05
CdCO ₃ , ZnCO ₃ , CuCO ₃ , PbCO ₃ , CdO, PbO, ZnO, Cu ₂ O	secondary mineral	

Compositions taken from HSC Sim tails output

Table S7. Initial composition of tailings from skarn deposit

Mineral	Content	
	Wt %	(mole/kg)
Calcite	1.26E+01	1.26E+00
Chalcopyrite	1.65E-01	3.02E-02
Pyrite	5.90E+00	7.07E-01
Quartz	8.11E+01	4.87E+00
Ca(OH)2	1.80E-01	1.33E-02
Cd(OH)2	6.22E-04	9.10E-05
Zn(OH)2	4.51E-02	4.51E-03
Pb(OH)2	2.27E-03	5.48E-04
Cu(OH)2	2.50E-02	2.44E-03
As, on hydroxide sites	4.63E-04	6.17E-06
CdCO ₃ , ZnCO ₃ , CuCO ₃ , PbCO ₃ , CdO, PbO, ZnO, Cu ₂ O	secondary mineral	

Compositions taken from HSC Sim tails output

Table S8. Initial composition of tailings from sediment hosted deposit

Mineral	Content	
	Wt %	(mole/kg)
Calcite	1.47E+01	1.47E+00
Chalcopyrite	7.02E-01	1.29E-01
Galena	2.63E+00	6.31E-01
Marcasite	3.74E+00	4.49E-01
Pyrite	9.88E+00	1.18E+00
Quartz	6.50E+01	3.90E+00
Sphalerite	2.72E+00	2.64E-01
$\text{Ca}(\text{OH})_2$	1.60E-01	1.18E-02
$\text{Cd}(\text{OH})_2$	6.11E-03	8.94E-04
$\text{Zn}(\text{OH})_2$	4.39E-01	4.39E-02
$\text{Pb}(\text{OH})_2$	2.78E-03	6.70E-04
$\text{Cu}(\text{OH})_2$	6.11E-03	5.96E-04
As, on hydroxide sites	4.97E-03	6.62E-05
CdCO_3 , ZnCO_3 , CuCO_3 , PbCO_3 , CdO , PbO , ZnO , Cu_2O	secondary mineral	

Compositions taken from HSC Sim tails output

Table S9. Initial composition of tailings from magmatic sulfide deposit

Mineral	Content	
	Wt %	(mole/kg)
Calcite	7.29E+00	7.29E-01
Chalcopyrite	1.76E-01	3.22E-02
Galena	1.06E+01	2.54E+00
Pyrite	5.00E+00	5.99E-01
Quartz	7.20E+01	4.32E+00
Sphalerite	4.83E+00	4.69E-01
$\text{Ca}(\text{OH})_2$	1.20E-01	8.88E-03
$\text{Cd}(\text{OH})_2$	1.97E-03	2.89E-04
$\text{Zn}(\text{OH})_2$	4.64E-02	4.64E-03
$\text{Pb}(\text{OH})_2$	6.94E-04	1.67E-04
$\text{Cu}(\text{OH})_2$	1.53E-03	1.49E-04
As, on hydroxide sites	1.56E-05	2.08E-07
CdCO_3 , ZnCO_3 , CuCO_3 , PbCO_3 , CdO , PbO , ZnO , Cu_2O	secondary mineral	

Compositions taken from HSC Sim tails output

Table S10. Initial composition of tailings from iron oxide deposit

Mineral	Content	
	Wt %	(mole/kg)
Calcite	1.30E+01	1.30E+00
Chalcopyrite	2.44E-01	4.47E-02
Pyrite	2.97E+00	3.56E-01
Quartz	8.36E+01	5.01E+00
Ca(OH)2	1.20E-01	8.88E-03
Cd(OH)2	2.17E-03	3.18E-04
Zn(OH)2	7.86E-02	7.86E-03
Pb(OH)2	2.35E-04	5.68E-05
Cu(OH)2	2.12E-03	2.07E-04
As, on hydroxide sites	1.77E-03	2.35E-05
CdCO ₃ , ZnCO ₃ , CuCO ₃ , PbCO ₃ , CdO, PbO, ZnO, Cu ₂ O	secondary mineral	

Compositions taken from HSC Sim tails output

Table S11. Initial composition of tailings from intrusion related deposit

Mineral	Content	
	Wt %	(mole/kg)
Calcite	1.06E+01	1.06E+00
Chalcopyrite	1.53E-01	2.80E-02
Pyrite	2.91E+00	3.49E-01
Quartz	8.62E+01	5.17E+00
Ca(OH)2	1.50E-01	1.11E-02
Cd(OH)2	9.78E-04	1.43E-04
Zn(OH)2	5.26E-02	5.26E-03
Pb(OH)2	1.28E-04	3.10E-05
Cu(OH)2	1.33E-03	1.29E-04
As, on hydroxide sites	1.21E-03	1.61E-05
CdCO ₃ , ZnCO ₃ , CuCO ₃ , PbCO ₃ , CdO, PbO, ZnO, Cu ₂ O	secondary mineral	

Compositions taken from HSC Sim tails output

Table S12. Initial composition of tailings from epithermal deposit

Mineral	Content	
	Wt %	(mole/kg)
Calcite	5.87E+00	5.87E-01
Chalcopyrite	1.65E-01	3.03E-02
Galena	5.44E+00	1.31E+00
Pyrite	1.03E+01	1.23E+00
Quartz	7.72E+01	4.63E+00
Sphalerite	4.00E-01	3.88E-02
$\text{Ca}(\text{OH})_2$	1.10E-01	8.14E-03
$\text{Cd}(\text{OH})_2$	5.96E-03	8.73E-04
$\text{Zn}(\text{OH})_2$	1.52E-01	1.52E-02
$\text{Pb}(\text{OH})_2$	2.77E-01	6.69E-02
$\text{Cu}(\text{OH})_2$	8.94E-02	8.72E-03
As, on hydroxide sites	2.37E-03	3.16E-05
CdCO ₃ , ZnCO ₃ , CuCO ₃ , PbCO ₃ , CdO, PbO, ZnO, Cu ₂ O	secondary mineral	

Compositions taken from HSC Sim tails output

Table S13. Geochemical thermodynamic reactions included in the simulation from PHREEQC database³⁷ and WATEQ4F database³⁰

Solid phases (bold letters)	
Chemical equilibrium of precipitation / dissolution reactions	$\log K_{s0}$
CaCO₃ = Ca ²⁺ + CO ₃ ²⁻	-8.48
CaSO_{4.2H₂O} = Ca ²⁺ + SO ₄ ²⁻ + 2 H ₂ O	-4.58
Ca(OH)₂ + 2 H ⁺ = Ca ²⁺ + 2 H ₂ O	22.8
Cd(OH)₂ + 2 H ⁺ = Cd ²⁺ + 2 H ₂ O	20.19
Zn(OH)₂ + 2 H ⁺ = Zn ²⁺ + 2 H ₂ O	17.82
Cu(OH)₂ + 2 H ⁺ = Cu ²⁺ + 2 H ₂ O	16.2
Pb(OH)₂ + 2 H ⁺ = Pb ²⁺ + 2 H ₂ O	16.94
Al(OH)₃ + 3 H ⁺ = Al ³⁺ + 3 H ₂ O	8.11
CuCO₃ = Cu ²⁺ + CO ₃ ²⁻	-9.63
ZnCO₃ = Zn ²⁺ + CO ₃ ²⁻	-10.0
CdCO₃ = Cd ²⁺ + CO ₃ ²⁻	-12.1
PbCO₃ = Pb ²⁺ + CO ₃ ²⁻	-13.1
CdO + 2 H ⁺ = Cd ²⁺ + H ₂ O	13.8
PbO + 2 H ⁺ = Pb ²⁺ + H ₂ O	12.9
ZnO + 2 H ⁺ = Zn ²⁺ + H ₂ O	11.1
Arsenic complexation on HFO ³⁵	
Acid base reactions	
AsO ₄ ³⁻ + H ⁺ = HAsO ₄ ²⁻	11.6
AsO ₄ ³⁻ + 2H ⁺ = H ₂ AsO ₄ ⁻	18.35
AsO ₄ ³⁻ + 3H ⁺ = H ₃ AsO ₄	20.6
Surface reactions	
SurfOH + H ⁺ = SurfOH ₂ ⁺	7.29
SurfOH = SurfO ⁻ + H ⁺	-8.93
SurfOH + AsO ₄ ³⁻ + 3H ⁺ = SurfH ₂ AsO ₄ + H ₂ O	29.31
SurfOH + AsO ₄ ³⁻ + 2H ⁺ = SurfHAsO ₄ ⁻ + H ₂ O	23.51
SurfOH + AsO ₄ ³⁻ = SurfOHAsO ₄ ³⁻	10.58

The following figures show the model output of simulations for the various types of tailings.

It can be seen that some metals like Zn and Cu (and partially Pb) in the leachate surpass threshold concentrations and hence represent a risk to the environment. We also display the threshold values in Figure S6-Figure S13, taken from EU groundwater leachate discharge values⁴⁷.

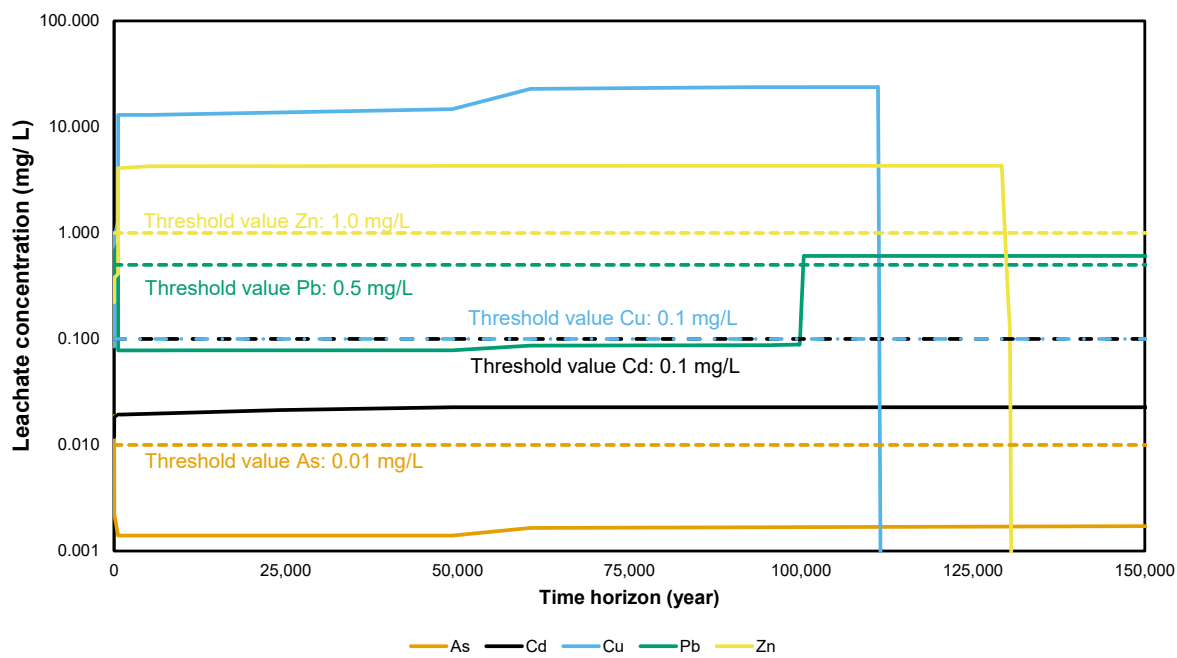


Figure S6. Porphyry tailings: Modeled leachate concentrations of As, Cd, Cu, Pb and Zn, according to the geochemical model up to 150k years after disposal of porphyry tailings. EU groundwater leachate discharge threshold values⁴⁷ are displayed for comparison

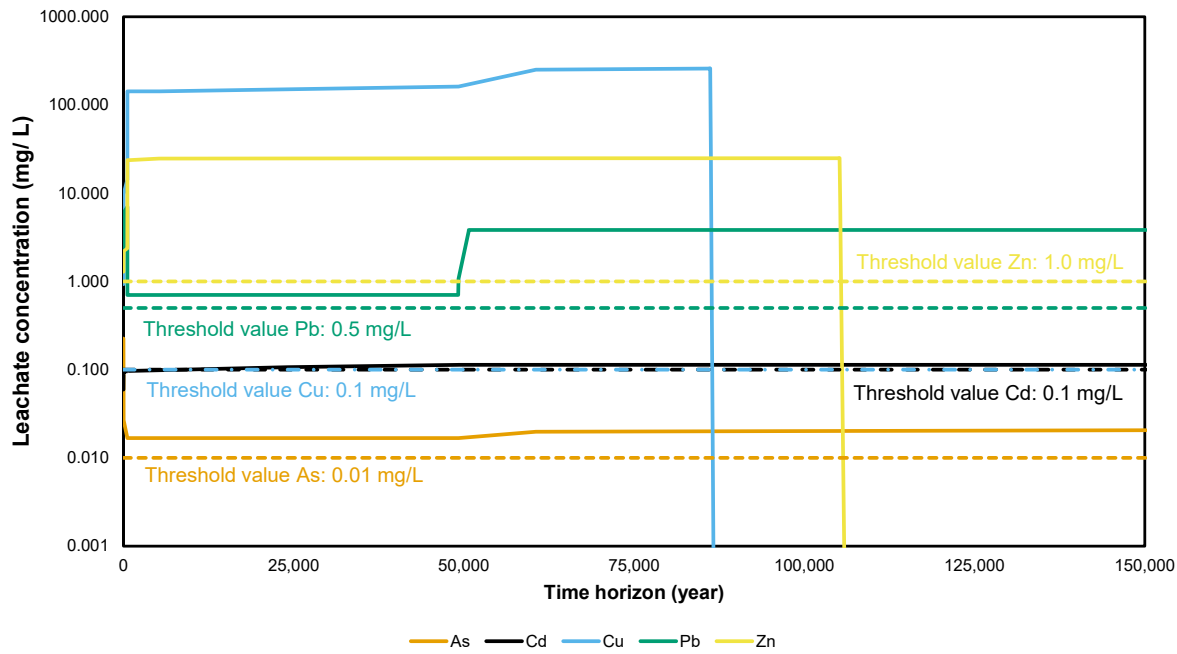


Figure S7. Volcanogenic massive sulfide tailings: Modeled leachate concentrations of As, Cd, Cu, Pb and Zn, according to the geochemical model up to 150k years after disposal of volcanicogenic massive sulfide tailings. EU groundwater leachate discharge threshold values⁴⁷ are displayed for comparison

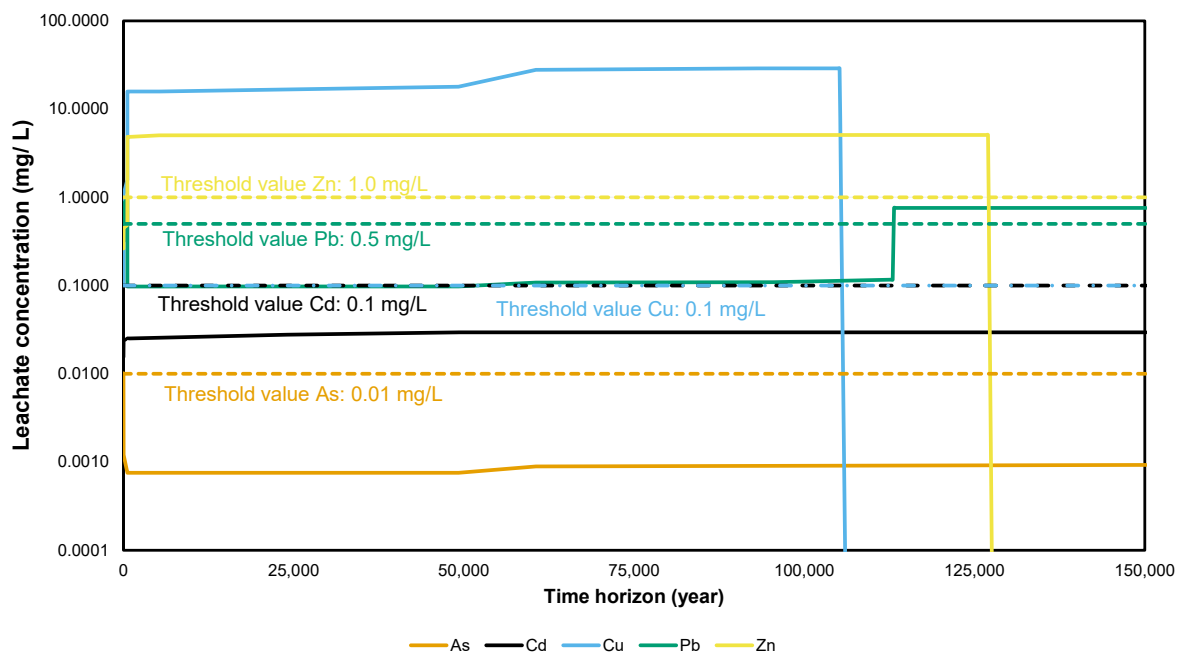


Figure S8. Skarn tailings: Modeled leachate concentrations of As, Cd, Cu, Pb and Zn, according to the geochemical up to 150k years after disposal of skarn tailings. EU groundwater leachate discharge threshold values⁴⁷ are displayed for comparison

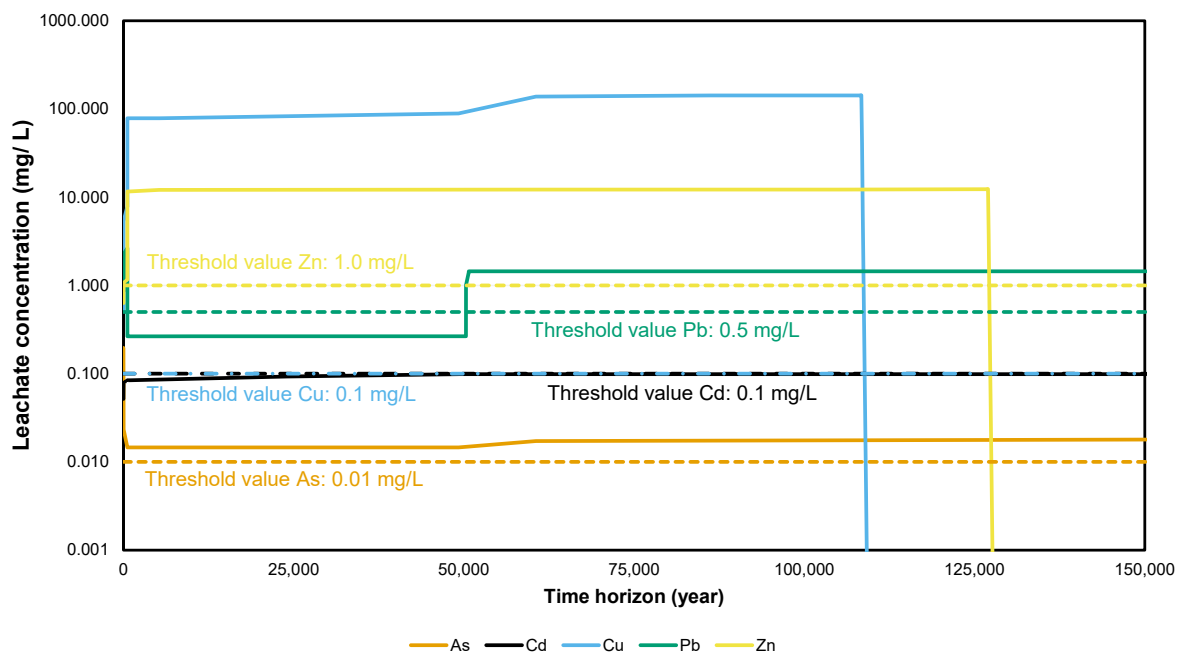


Figure S9. Sediment hosted tailings: Modeled leachate concentrations of As, Cd, Cu, Pb and Zn, according to the geochemical up to 150k years after disposal of sediment hosted tailings. EU groundwater leachate discharge threshold values⁴⁷ are displayed for comparison

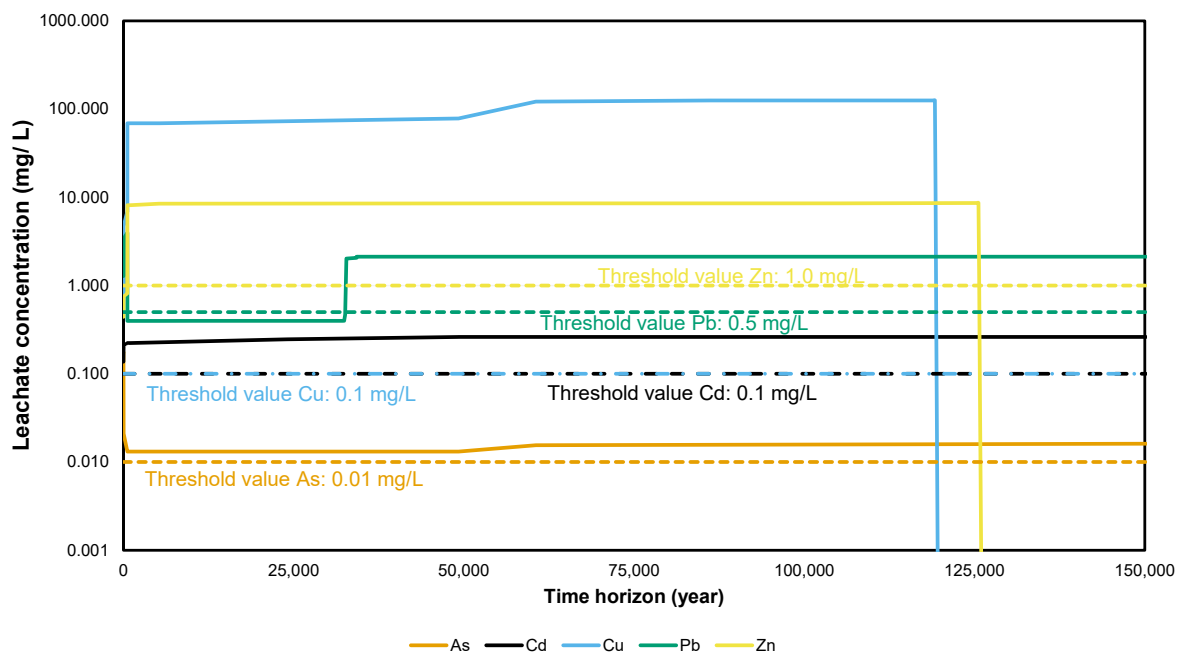


Figure S10. Magmatic sulfide tailings: Modeled leachate concentrations of As, Cd, Cu, Pb and Zn, according to the geochemical up to 150k years after disposal of magmatic sulfide tailings. EU groundwater leachate discharge threshold values⁴⁷ are displayed for comparison

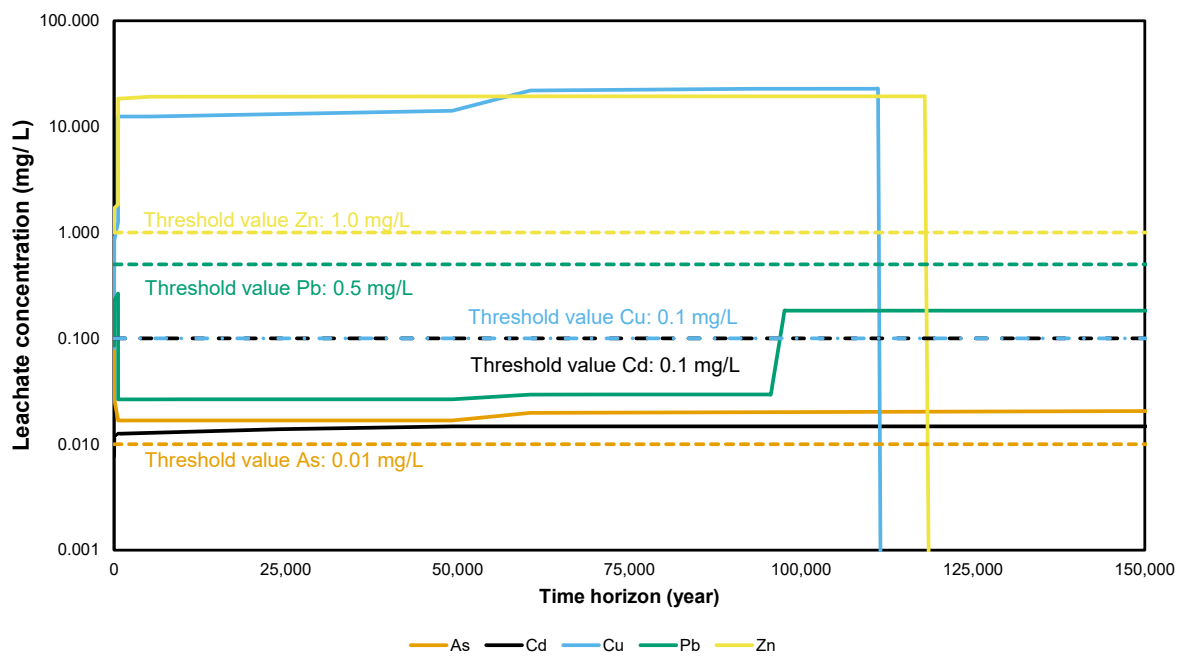


Figure S11. Iron oxide tailings: Modeled leachate concentrations of As, Cd, Cu, Pb and Zn, according to the geochemical up to 150k years after disposal of iron oxide tailings. EU groundwater leachate discharge threshold values⁴⁷ are displayed for comparison

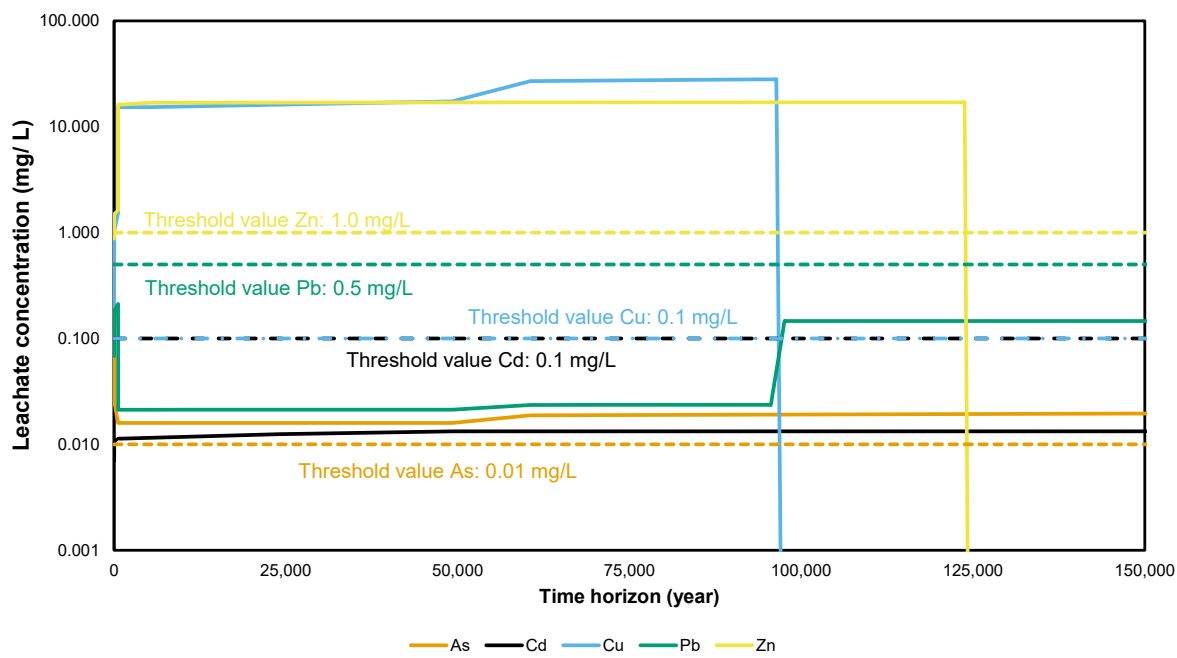


Figure S12. Intrusion-related tailings: Modeled leachate concentrations of As, Cd, Cu, Pb and Zn, according to the geochemical up to 150k years after disposal of intrusion-related tailings. EU groundwater leachate discharge threshold values⁴⁷ are displayed for comparison

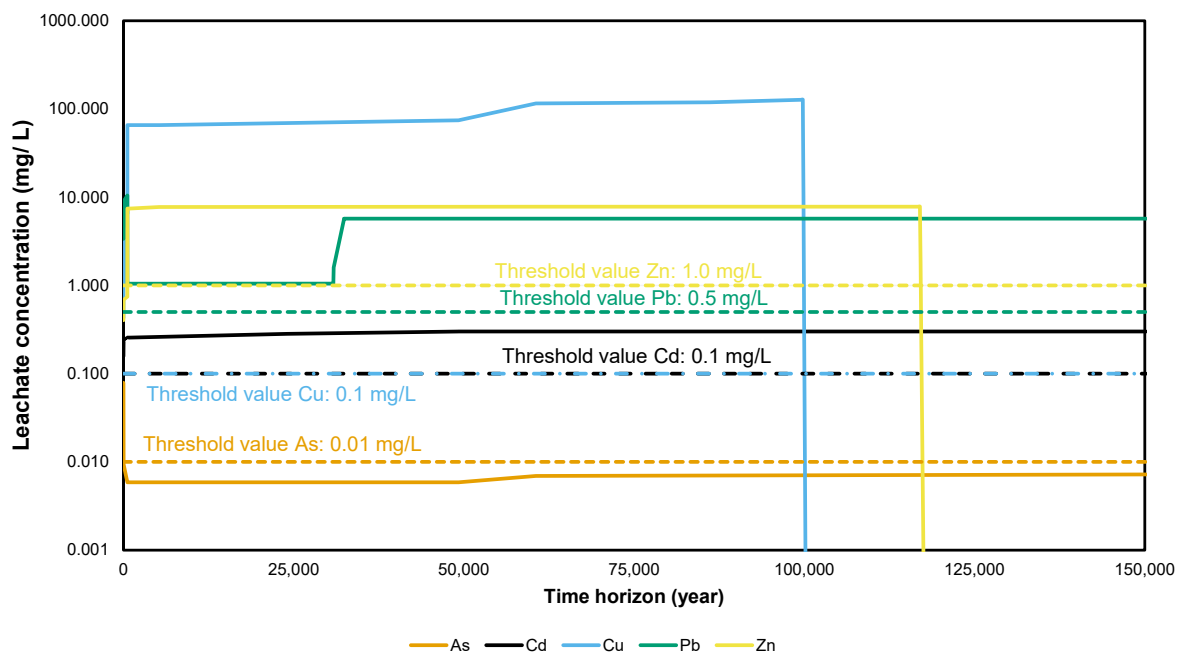


Figure S13. Epithermal tailings: Modeled leachate concentrations of As, Cd, Cu, Pb and Zn, according to the geochemical up to 150k years after disposal of epithermal tailings. EU groundwater leachate discharge threshold values⁴⁷ are displayed for comparison

S6. Net infiltration map (groundwater recharge) using GLOBWB model

To account for site-specific net infiltrations, we took the values from PCR GLOBWB^{48,49} (for further descriptions, check the mentioned references). The schematic water flows and the annual net infiltration (or groundwater recharge) map are displayed in Figure S14.

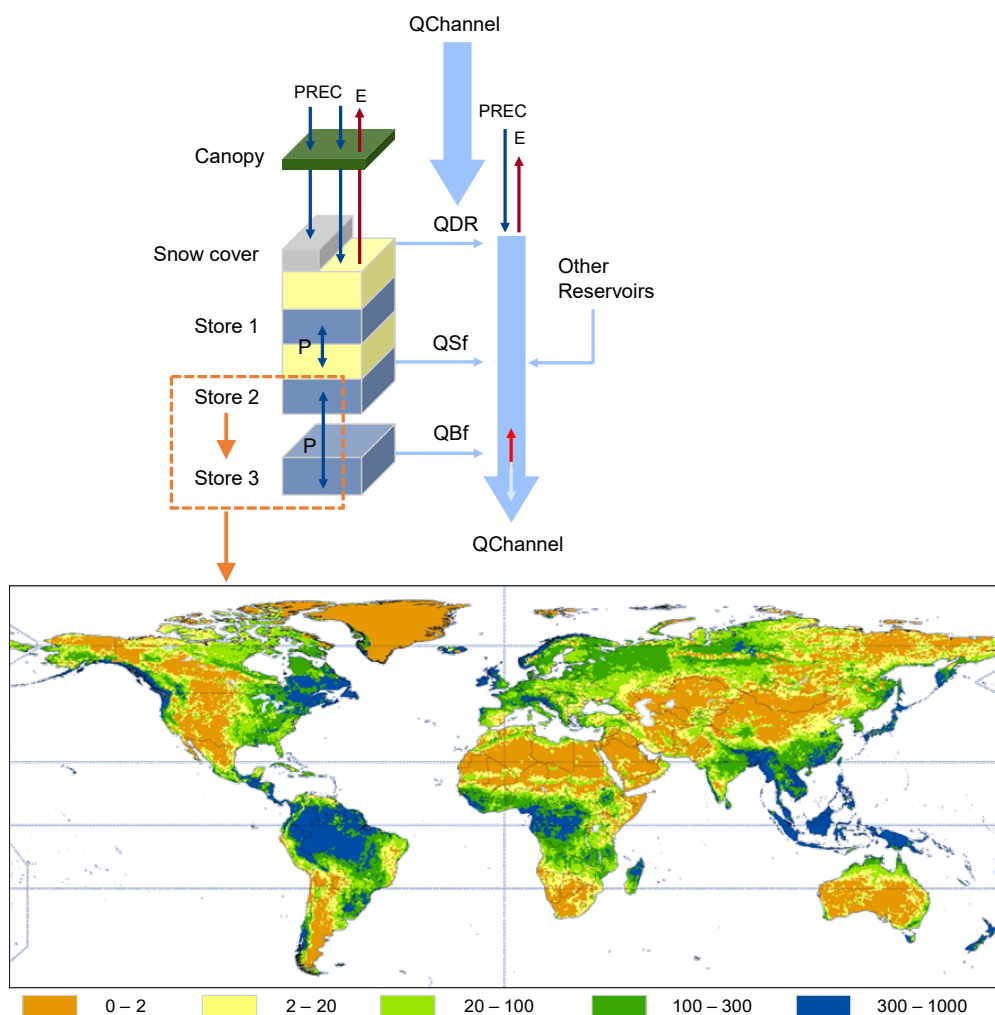


Figure S14. Top: The conceptual water flows in PCR-GLOBWB, redrawn from Sutanudjaja et al.⁴⁸. Bottom: The annual groundwater recharge, taken from the results of PCR-GLOBWB in mm per year^{48,49}. Abbreviations: PREC= Precipitation, E= Evaporation, P= Percolation/ capillary rise, QDR= Direct run-off, QSf= Interflow or subsurface stormflow, QBf= Baseflow, QChannel= Discharge along the channel

S7. Baseline scenario: Environmental hotspots

This section explains how we derived the grouping of datasets and performed global LCA for copper tailings. The gray area in Figure S15 is the focus of this study, where we want to improve the granularity of tailings disposal dataset before they are matched with the other downstream processes (indicated in orange area). Due to difference in resolutions, we classified the datapoints ($n = 431$) of tailings disposal with the other six datasets that represent copper smelter/ refinery processes across the world. Meanwhile, Figure S16 shows how we grouped the simulated results in our study and eventually the basis of comparison in Figure 5 in the main paper.

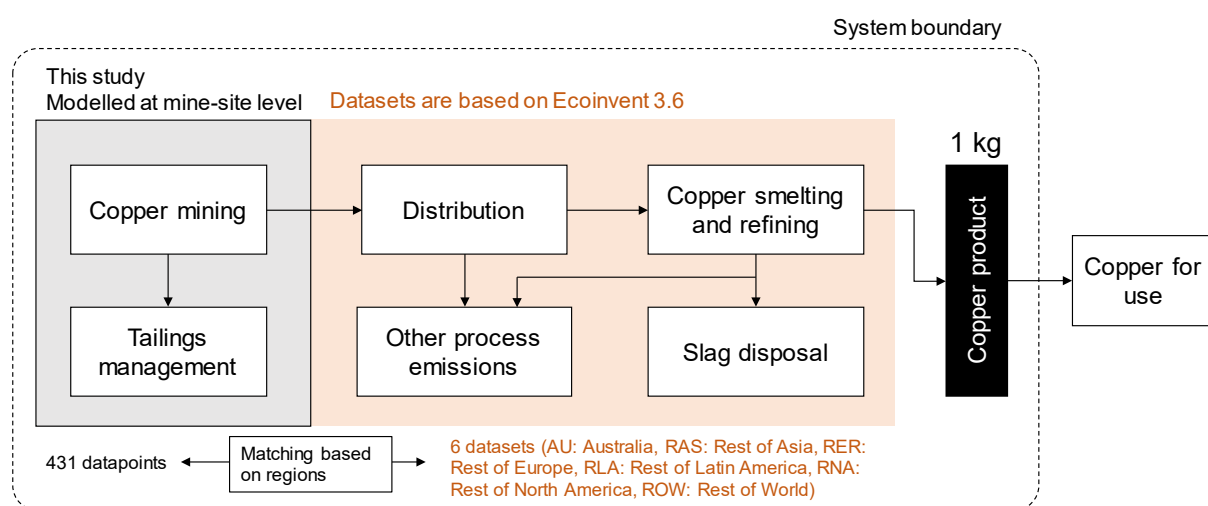


Figure S15. LCA system boundary to produce 1 kg copper

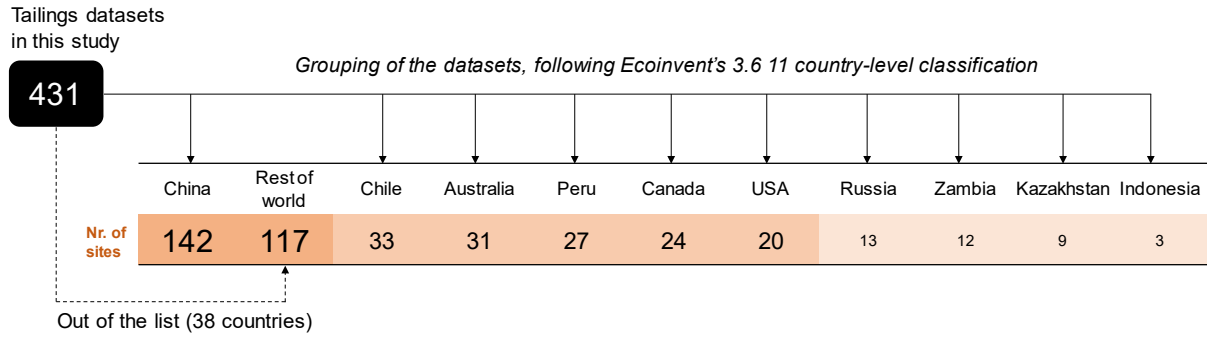
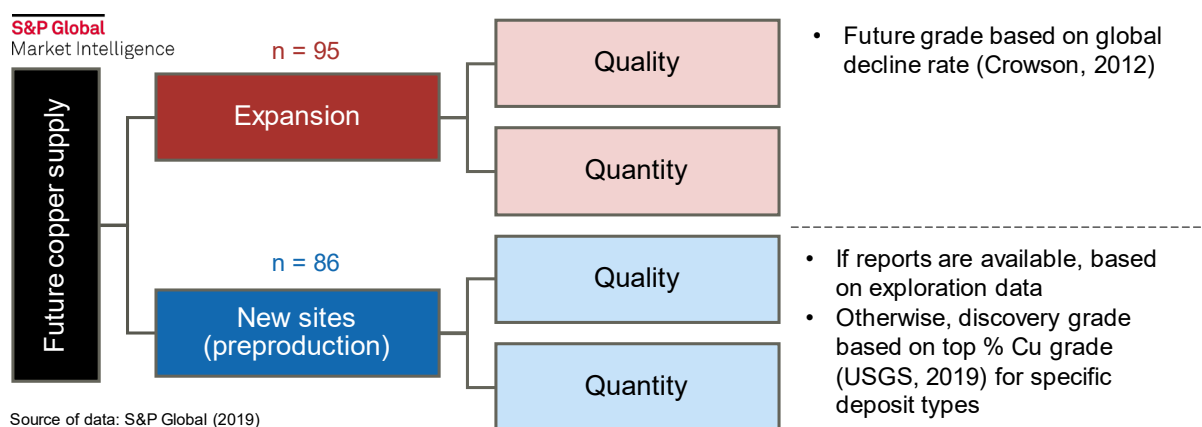


Figure S16. The procedure to systematically compare generated tailings inventory data (this study) with the available ones in LCA database

S8. Primary copper production data for 2019 – 2050

The data for copper supply up to mid of the 21st century are mainly collected from Elshkaki et al. and Northey at al. studies^{50–52}. Where gaps are found, we used assumptions to estimate the volume of copper produced in respective countries by subtraction. In addition to complete descriptions of this approach in the main paper, here we presented in Figure S17 and Figure S18 the schematic of our study scopes.



$$\text{Primary supply}_{\text{year } t} = \sum \text{Primary supply}_{\text{year } t-1} + \sum (\text{Supply expansion} + \text{New expansion})_{\text{year } t}$$

Figure S17. Future copper supply estimation and data compilation

In this study, we considered only the preproduction as the data already represent sites with higher certainty to supplying copper. However, three preproduction categories were obtained from the market intelligence platform⁵ that indicates the active operational phase:

- Commissioning, hence, it will be active in 1 year
- Construction stages. In these subcases, we assumed it will take 3 years for those already in track while it will take 5 years for those sites in plan. Further details can be seen in the Supporting Information-2, S2.7 – S2.8 (i.e., the list of all projects, including site expansion: 95 sites and new site opening: 86 sites).

Based on the latest available data on S&P Market Intelligence⁵, we narrowed down the future copper sites on phase 2 and 3 (see Figure S18). The data on this platform is somewhat limited to account for abandoned sites and the appearance of sites with its copper throughputs. Therefore, we ultimately merged the data gathered from this online source with the other forecasting studies^{50–52} to obtain complete information for future supplies.

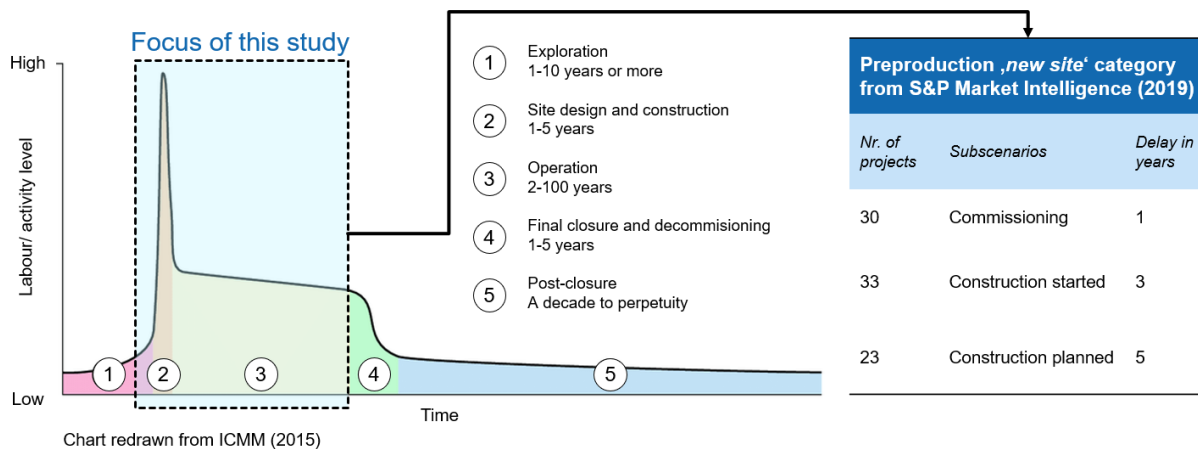


Figure S18. The cases for preproduction sites with three different categories of greenfield mining. Adapted after ICMM⁵³

S9. Freshwater ecotoxicity impacts from baseline year 2019 to 2050

Table S14. Summary of results for the ecotoxicity projection from 2019 to 2050 in all countries (Unit: CTUe per year, method: USETox)

Cases	Argentina	Armenia	Australia	Azerbaijan	Bolivia	Botswana	Brazil	Bulgaria	Canada	Chile	China	Colombia	Cyprus	Dem. Rep. Congo	Dominican Republic	Other countries	TOTAL all countries	% - changes relative to baseline	Effect of demand growth	Effect of ore decline
Ecoinvent 3.6 (2019)	1.20E+11	2.10E+11	3.38E+12	7.46E+09	6.83E+09	1.64E+10	1.72E+12	6.52E+11	2.74E+12	2.58E+13	5.48E+12	1.29E+10	2.60E+10	1.98E+12	2.46E+10	...	8.50E+13	124%		
This study (2019)	1.98E+10	2.65E+10	2.38E+12	8.36E+09	6.61E+09	1.92E+10	1.84E+12	1.68E+11	3.92E+12	6.39E+12	3.12E+12	7.43E+10	4.92E+09	5.72E+12	5.22E+10	...	6.83E+13	100%		
2030 - same ore grade	5.98E+09	8.00E+09	3.89E+12	2.53E+09	2.00E+09	5.79E+09	1.38E+12	5.08E+10	2.93E+12	1.15E+13	6.03E+12	2.25E+10	1.49E+09	8.78E+12	1.58E+10	...	1.14E+14	87%		
2030 - with ore grade decline	6.85E+09	9.16E+09	4.46E+12	2.89E+09	2.29E+09	6.63E+09	1.58E+12	5.82E+10	3.36E+12	1.32E+13	6.91E+12	2.57E+10	1.70E+09	1.01E+13	1.81E+10	...	1.31E+14	192%	13%	
2040 - same ore grade	1.78E+10	2.39E+10	4.15E+12	7.54E+09	5.96E+09	1.73E+10	1.77E+12	1.52E+11	3.76E+12	1.15E+13	4.49E+12	6.70E+10	4.43E+09	5.49E+12	4.71E+10	...	9.61E+13	77%		
2040 - with ore grade decline	2.31E+10	3.09E+10	5.38E+12	9.77E+09	7.72E+09	2.24E+10	2.29E+12	1.97E+11	4.87E+12	1.49E+13	5.82E+12	8.69E+10	5.75E+09	7.11E+12	6.11E+10	...	1.25E+14	182%	23%	
2050 - same ore grade	1.71E+10	2.28E+10	4.12E+12	7.21E+09	5.70E+09	1.65E+10	1.69E+12	1.45E+11	3.59E+12	1.08E+13	2.55E+12	6.41E+10	4.24E+09	5.25E+12	4.50E+10	...	7.43E+13	68%		
2050 - with ore grade decline	2.50E+10	3.34E+10	6.03E+12	1.06E+10	8.35E+09	2.42E+10	2.48E+12	2.12E+11	5.27E+12	1.59E+13	3.74E+12	9.39E+10	6.21E+09	7.69E+12	6.60E+10	...	1.09E+14	159%	32%	
																See SI for complete list	Value for demand growth = Sum without decline divided by sum with ore grade decline	Value = 100% – effect of demand growth		

*Other results are available in the SI-2 document (S2.6a supply projection and S2.6b the exhaustive table with all countries)

S10. Compare tailings characteristics from model prediction vs. tailings characteristics from actual data

We compared tailings characteristics from model prediction vs. tailings characteristics from actual data (on-site, taken from an operating facility⁴⁵). The results of the sensitivity analysis for low efficiency and high efficiency in ore beneficiation are also presented in both Table S15 and Figure S19.

Table S15. Comparison of approximated results for three flotation cases vs. plant data

Metals (in mg/ kg)	Simulated			Plant data				Average	% diff with low	% diff with base	% diff with high
	Low limit Hi- efficiency	Base	High limit Lo-efficiency	Tailings sample A	Tailings sample B	Tailings sample C	Average				
Zn	5,269	8,130	11,019	7,400	10,529	8,535	8,821	-67%	-8%	20%	
Cu	2,815	4,436	6,005	6,600	4,721	4,480	5,267	-87%	-19%	12%	
As	2,424	3,819	5,170	5,095	4,073	4,952	4,707	-94%	-23%	9%	
Pb	1,379	2,528	3,603	2,500	5,896	3,300	3,899	-183%	-54%	-8%	
Cd	18	29	39	NA	31	NA	31	-70%	-8%	20%	

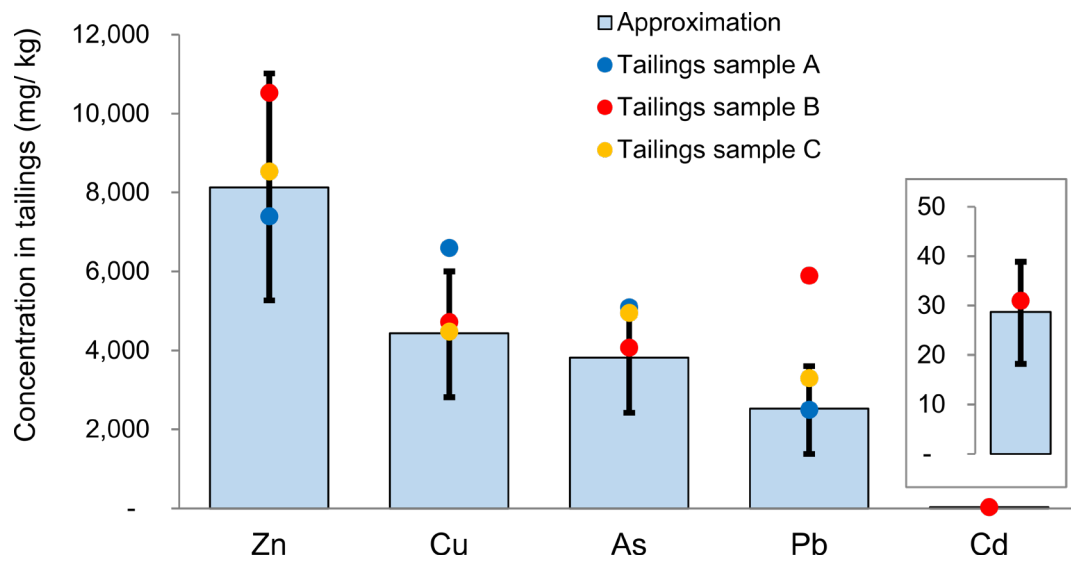


Figure S19. Comparison of metal compositions from simulated results vs. collected data from mining partners. The upper limit of the whisker represents worst case with worse flotation performance, and the lower limit represents better flotation performance.

We additionally conducted comparative analysis of tailings composition from our model vs. data from field measurements in Chilean tailings. For that, we rely on the compilation of data by the Chilean Geological Survey ‘SERNAGEOMIN’⁵⁴, which provide data for heavy metal compositions of major sites in Chile. Two sites, namely Escondida and Los Pelambres were chosen as cases because of the data availability ($n > 2$). Copper and cadmium, among other heavy metals, have a large variability even in a single site due to multiple factors^{55,56}: ore deposits, location of sampling, weathering, and other uncertainties in the data collection. The sensitivity in the model input also shows that while there is disparity between simulation and reality, the values are generally in good agreement within the same order of magnitude. However, more validations are still needed to confirm this finding for other sites and, in the same line, for recognizing uncertainties within input characteristics and tailings/ ore deposit geochemistry.

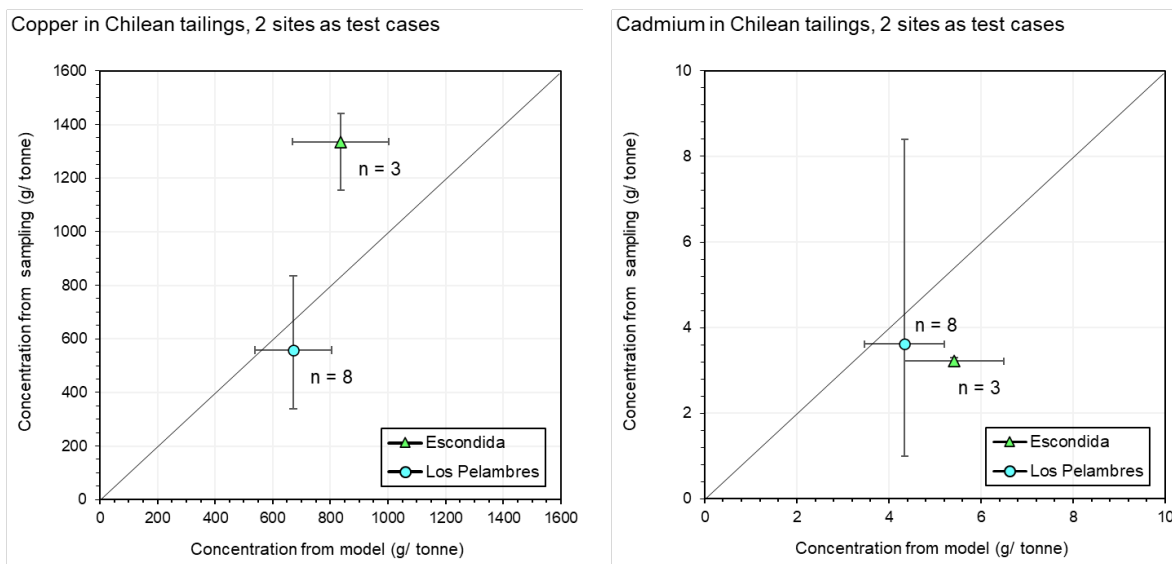


Figure S20. Comparison of metal compositions from simulated results x-axis vs. tailings data from Chilean sites y-axis. Blue circles represent results from base calculation, while green triangles are averaged sampling data from survey. Whiskers represent the highest and lowest value in the dataset (vertical) and simulated results (horizontal), respectively.

In average, copper yield in the beneficiations is ranging from 80 – 95% from our simulations. As concluding remarks, improving flotation processes in general^{57,58} is a must when the yield is comparably lower according to the previously mentioned range. However, the efficiency of

flotation in general is already reaching the mature performance according to the literature, even in the last couple of decades, so the efficiency can only improve slightly by upgrading the beneficiation facility⁵⁹.

S11. Aggregated results for long term horizon

Table S16 contains aggregated freshwater ecotoxicity results caused by tailings deposition, in a long-term perspective (60,000 years). In addition, we also presented a graphical representation of this result in Figure S21 as tree map chart for a hi-level overview.

Table S16. The summary of aggregated freshwater ecotoxicity (long-term horizon) results in this study. The data is also derived from previous figures.

Continents	Country	Aggregated Freshwater Eco-toxicity (CTUe)	Contribution
<i>Africa</i>	Dem. Rep. Congo	5.72E+12	8%
<i>Africa</i>	Zambia	4.83E+12	7%
<i>Africa</i>	Morocco	1.56E+11	0%
<i>Africa</i>	South Africa	7.41E+10	0%
<i>Africa</i>	Mauritania	4.13E+09	0%
<i>Africa</i>	Eritrea	4.29E+10	0%
<i>Africa</i>	Namibia	2.02E+10	0%
<i>Africa</i>	Zimbabwe	2.77E+10	0%
<i>Africa</i>	Botswana	1.92E+10	0%
<i>Asia and Oceania</i>	Australia	2.38E+12	3%
<i>Asia and Oceania</i>	China	3.12E+12	5%
<i>Asia and Oceania</i>	Indonesia	3.99E+12	6%
<i>Asia and Oceania</i>	Kazakhstan	9.67E+11	1%
<i>Asia and Oceania</i>	Mongolia	1.06E+10	0%
<i>Asia and Oceania</i>	Iran	4.58E+10	0%
<i>Asia and Oceania</i>	Laos	5.86E+11	1%
<i>Asia and Oceania</i>	Papua New Guinea	5.80E+11	1%
<i>Asia and Oceania</i>	Saudi Arabia	1.11E+10	0%
<i>Asia and Oceania</i>	Uzbekistan	1.36E+10	0%
<i>Asia and Oceania</i>	Philippines	2.83E+11	0%
<i>Asia and Oceania</i>	India	4.27E+10	0%
<i>Asia and Oceania</i>	Myanmar	8.34E+10	0%
<i>Asia and Oceania</i>	Kyrgyzstan	6.99E+08	0%
<i>Asia and Oceania</i>	Pakistan	4.36E+09	0%
<i>Europe</i>	Russia	1.17E+13	17%
<i>Europe</i>	Poland	3.34E+12	5%
<i>Europe</i>	Spain	3.02E+12	4%
<i>Europe</i>	Portugal	7.40E+11	1%
<i>Europe</i>	Finland	5.40E+11	1%
<i>Europe</i>	Turkey	1.22E+11	0%
<i>Europe</i>	Bulgaria	1.68E+11	0%
<i>Europe</i>	Sweden	3.82E+11	1%
<i>Europe</i>	Georgia	3.30E+11	0%

<i>Europe</i>	Serbia	2.41E+10	0%
<i>Europe</i>	Armenia	2.65E+10	0%
<i>Europe</i>	Macedonia	2.64E+10	0%
<i>Europe</i>	Azerbaijan	8.36E+09	0%
<i>Europe</i>	Cyprus	4.92E+09	0%
<i>Europe</i>	Romania	1.92E+08	0%
<i>Latin America</i>	Chile	6.39E+12	9%
<i>Latin America</i>	Peru	9.23E+12	14%
<i>Latin America</i>	Mexico	7.67E+11	1%
<i>Latin America</i>	Brazil	1.84E+12	3%
<i>Latin America</i>	Colombia	7.43E+10	0%
<i>Latin America</i>	Dominican Republic	5.22E+10	0%
<i>Latin America</i>	Argentina	1.98E+10	0%
<i>Latin America</i>	Bolivia	6.61E+09	0%
<i>North America</i>	USA	2.56E+12	4%
<i>North America</i>	Canada	3.92E+12	6%
TOTAL		8.87E+13	6.83E+13

Note: Other results in different time horizons and human-toxicity impacts can be seen in the Supporting information-2.

Aggregated at higher level, Figure S21 shows how each continent's ecotoxicity contribution in a tree map-like chart. Obviously, Latin America leads due to the large production capacity and the amount of copper tailings being disposed. Europe and Africa, however, are ranked at the first and third despite having fewer copper site units and a limited number of copper-extracting countries. While this analysis is conducted for 2019, an in-depth discussion about future primary mining operations, especially for countries where ramping-up and brownfield sites are expected, is included in section 3.7.

2019 Toxicity of global copper tailings, Long-term emission

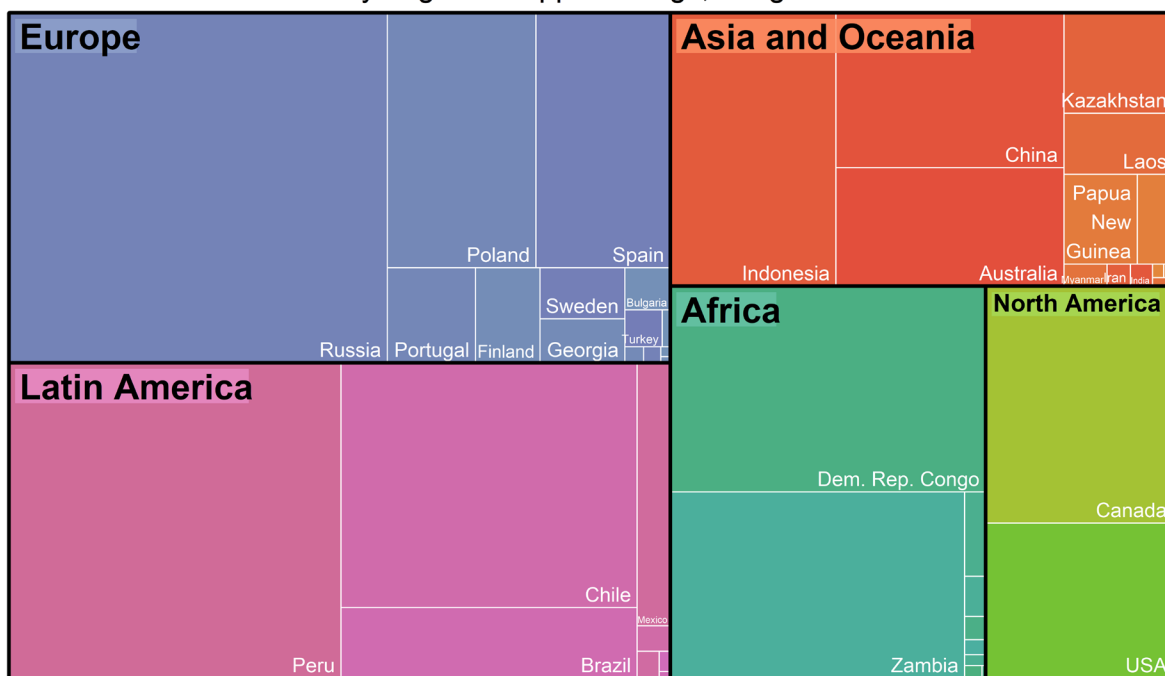


Figure S21. Contribution to global ecotoxicity impacts in 2019 per continent and country, illustrated in tree map chart. The area of each region and country is proportional to the estimated emissions.

S12. Impacts of climate conditions and ore deposit types (complementary results)

Figure S22 presents a boxplot chart to analyze the distribution of freshwater ecotoxicity across different deposit types and infiltration rates. Another way to see the results is shown in Figure S23, where we rank the highest toxicity results from the top based on median values of each group.

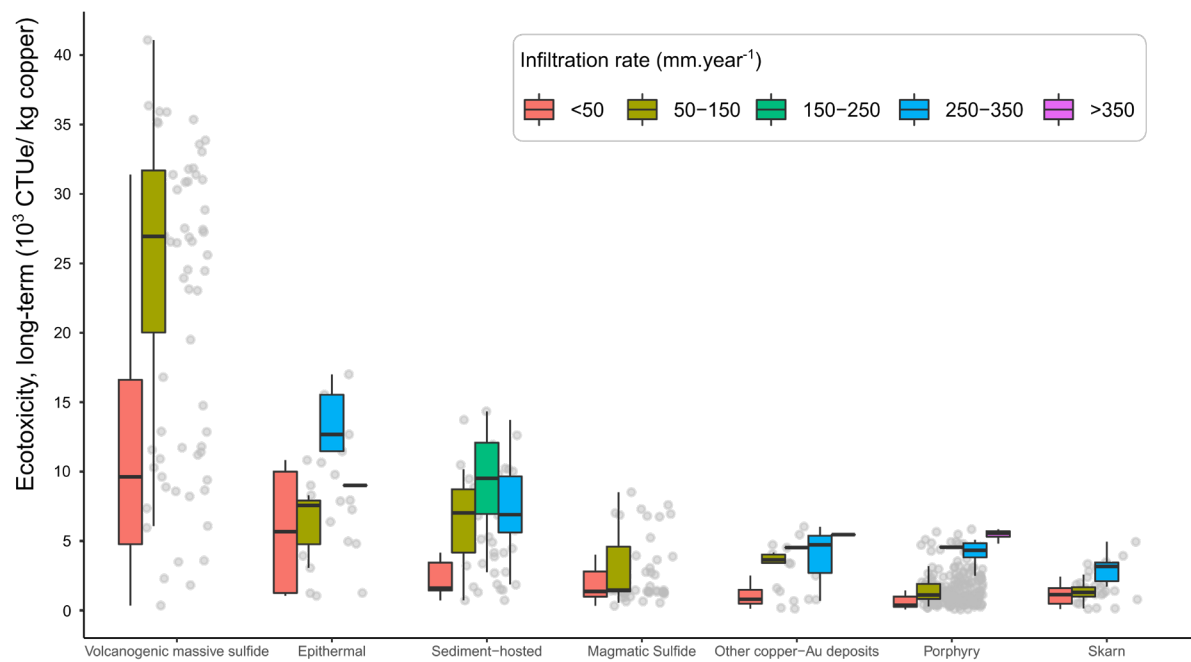


Figure S22. Distribution of ecotoxicity, grouped by net infiltration. The x-axis (copper deposit type) is ordered, based on the overall median of each class.

Moreover, we built two regression models below to see the influence of ore grades (Figure S24) and infiltration rate (Figure S25).

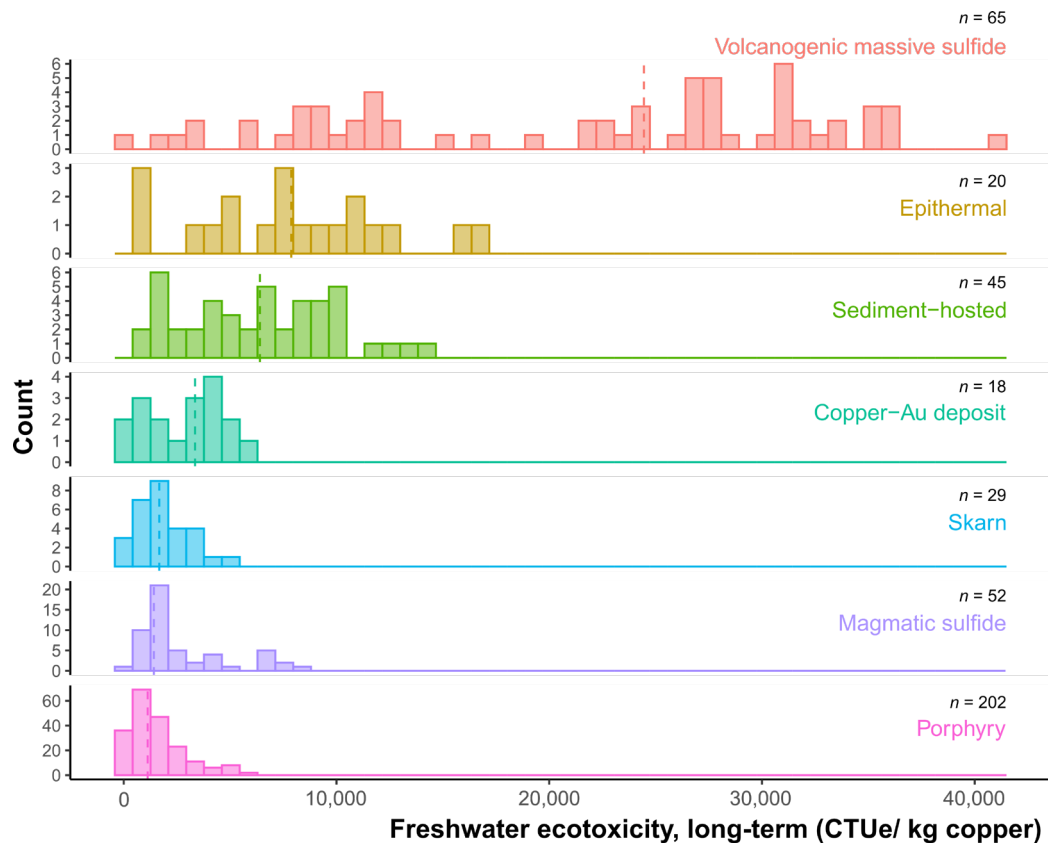


Figure S23. Histogram, shared x-axis (toxicity), grouped by deposit types. Dashed lines indicate median.

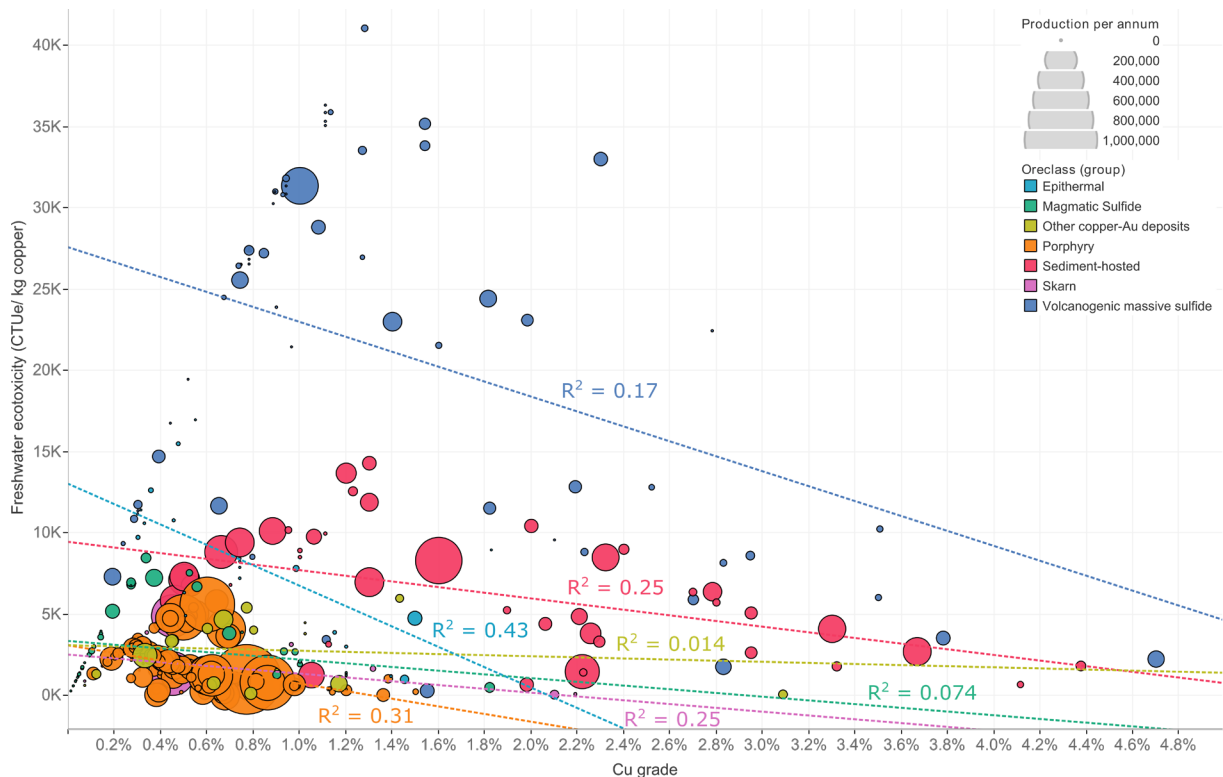


Figure S24. Regression Line, Cu grade vs. Toxicity per deposit type (left) and overall (right)

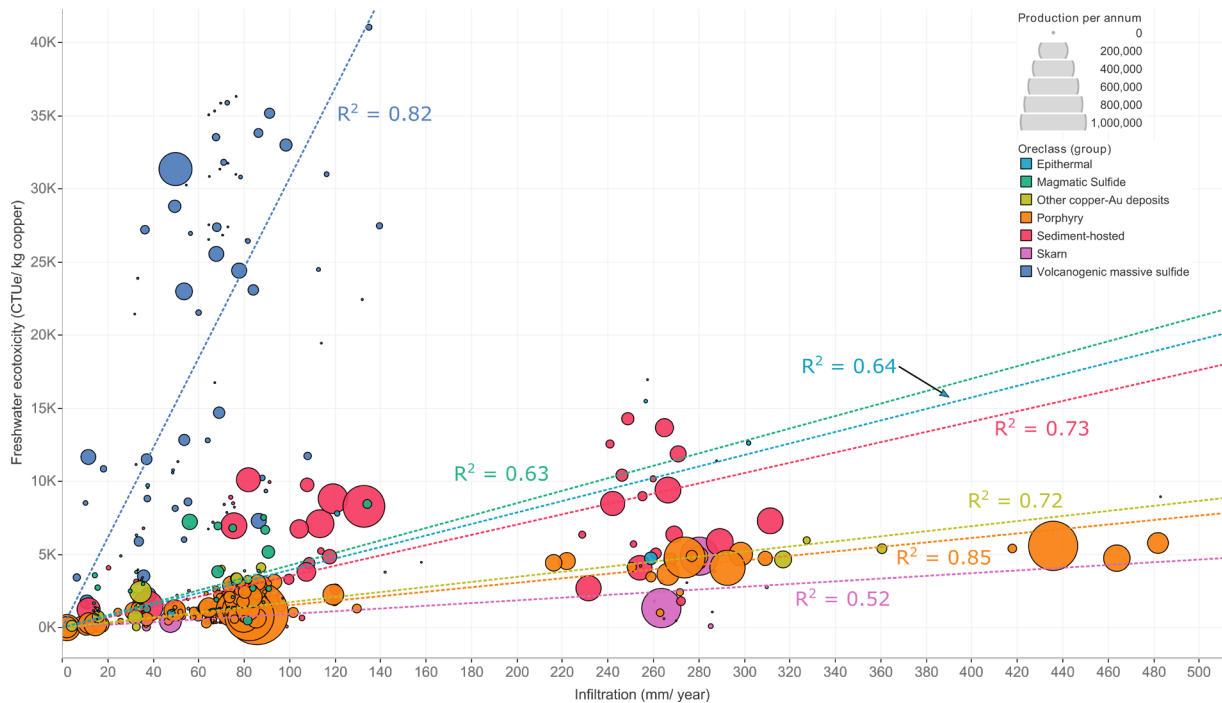


Figure S25. Scatter plots with regression lines: Net infiltration vs. Toxicity

Short summary of potential beneficiation upgrades:

Studies and field testing from sites have shown that flotation processes depend highly on the optimum size range of the ground ores, and is best represented by the “elephant curve”⁶⁰. This phenomenon describes that recovery of minerals follows an inverted U-shape curve, and it will suffer whenever the particle size entering flotation stage falls outside this recommended range. It is a well-recognized fact that flotation only works best when the floating particles can be liberated freely under ideal pulp-froth interactions, which in turn improve the area, kinetics, and overall recovery. In this study, the process simulator HSC Sim is set by default to minimize energy consumption in the single grinding stage at the upstream without maximizing the recovery of minerals. It implies that the single grinding stage will automatically lower its efforts to crush the higher-grade ore and as the consequence, it will also decrease the overall recovery⁶¹. We recognize this as one of the limitations in the mineral processing of our study. To overcome this setback, one can equip the standard copper

recovery circuits with advanced grinding techniques⁶² (i.e. installing multiple re-grinding stages to extend the liberation curve at optimum mineral recovery). However, this is usually not done to all common processes since we maintain standard copper recovery circuits in our simulations.

S13. Compiled copper production data for 2019

The main source of copper active sites are compiled from SNL Metal & Mining Market Intelligence data, study of Mudd et al., and USGS Mineral Deposits of the world (main features recorded: coordinates, tonnage, annual production capacity, and class of ore deposits)^{5,63,64}.

Table S17. Copper production from sulfides in 2019, compiled (only listed as an illustration in this document. For complete list, see Supporting Information-2)

Mine ID	Annual production (Mt)	Longitude	Latitude	Tonnage (economically mineable) in Mt	Cu-grade in %-w	Country	Continent	Ore deposit type
Escondida	904800	-69.1	-24.3	11,158.0	0.77%	Chile	Latin America	Porphyry
Collahuasi	559100	-68.7	-21.0	3,100.0	0.86%	Chile	Latin America	Porphyry
Grasberg	556557	137.2	-3.8	4,000.0	0.60%	Indonesia	Asia and Oceania	Porphyry
Cerro Verde	385818	-71.6	-16.5	2,528.0	0.50%	Peru	Latin America	Porphyry
El Teniente	320878	-70.5	-34.1	20,731.0	0.62%	Chile	Latin America	Porphyry
Morenci	129274	-109.4	33.1	6,470.0	0.52%	USA	North America	Porphyry
Las Bambas	285121	-72.3	-14.2	114.0	0.68%	Peru	Latin America	Porphyry
Los Bronces	284500	-70.3	-33.1	16,816.0	0.60%	Chile	Latin America	Porphyry
Los Pelambres	230240	-70.5	-31.7	7,458.0	0.62%	Chile	Latin America	Porphyry
Radomiro Tomic	232867	-68.9	-22.3	21,277.0	0.59%	Chile	Latin America	Porphyry
Chuquicamata	230936	-68.7	-21.0	3,100.0	0.86%	Chile	Latin America	Porphyry
Andina Division	131006	-70.5	-31.7	7,458.0	0.62%	Chile	Latin America	Porphyry
Spence	56448	-69.3	-22.8	497.0	0.92%	Chile	Latin America	Porphyry
Sarcheshmeh	120558	55.9	30.0	1,538.0	0.58%	Iran	Asia and Oceania	Porphyry
Toquepala	127200	-70.6	-17.2	2,320.0	0.55%	Peru	Latin America	Porphyry
Batu Hijau	161352	116.9	-9.0	1,640.0	0.44%	Indonesia	Asia and Oceania	Porphyry
Cuajone	112405	-70.7	-17.0	1,630.0	0.69%	Peru	Latin America	Porphyry
Oyu Tolgoi	159100	106.9	43.0	3,107.1	0.68%	Mongolia	Asia and Oceania	Porphyry
Centinela Sulfide	115070	-69.2	-23.2	519.0	0.41%	Chile	Latin America	Porphyry
...

Note: More exhaustive tables are provided in the spreadsheet of Supporting Information-2 (S2.1).

S14. Freshwater ecotoxicity results across continents and countries

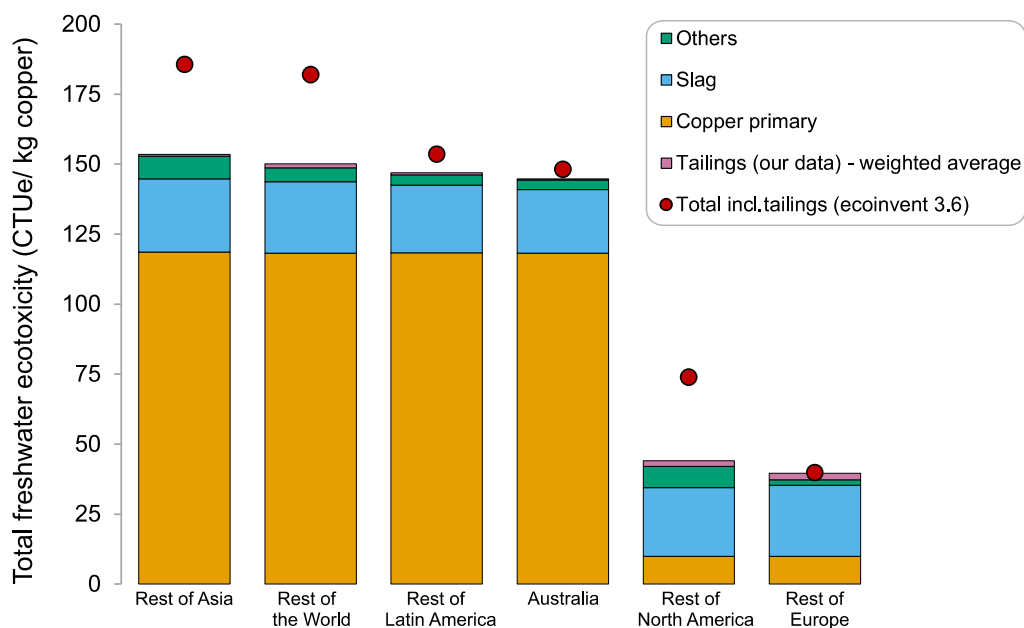
We aggregated the data at mine-site level to a continental-level by weighting the toxicity values (in CTUe, USEtox method) with the production capacity. The results for both short-term and long-term are presented in Table S18 and Figure S26. As for a more detailed analysis, the spread of toxicity at every mine site is included in the Supporting Information-2 (S2.10 – S2.11).

Table S18. Comparison of ecotoxicity (method: USEtox) results: Our study vs. Ecoinvent 3.6, aggregated following regions in the copper datasets

Short-term								
Region	Description	Tailings (our data) - weighted average	Tailings (ecoinvent 3.6)	Copper primary	Slag	Other processes	Total incl. tailings (Ecoinvent 3.6)	Total incl. tailings (our data)
AU	Australia	0	4	118	23	3	148	145
RAS	Rest of Asia	1	33	119	26	8	186	153
RER	Rest of Europe	2	3	10	25	2	40	40
RLA	Rest of Latin America	1	7	118	24	4	154	147
RNA	Rest of North America	2	32	10	25	8	74	44
ROW	Rest of World	1	33	118	26	5	182	150
Long-term								
Region	Description	Tailings (our data) - weighted average	Tailings (ecoinvent 3.6)	Copper primary	Slag	Other processes	Total incl. tailings (Ecoinvent 3.6)	Total incl. tailings (our data)
AU	Australia	2739	6596	118	54	86	6854	2997
RAS	Rest of Asia	3217	23084	119	62	107	23372	3505
RER	Rest of Europe	13359	2618	10	60	15	2703	13443
RLA	Rest of Latin America	2576	14256	118	57	81	14512	2832
RNA	Rest of North America	4764	25367	10	58	162	25597	4994
ROW	Rest of World	6052	15453	118	61	35	15666	6266

Note: The supporting information-2 (S2.10 – 11) document stores all the site-level results to obtain summarized values in this table.

(a)



(b)

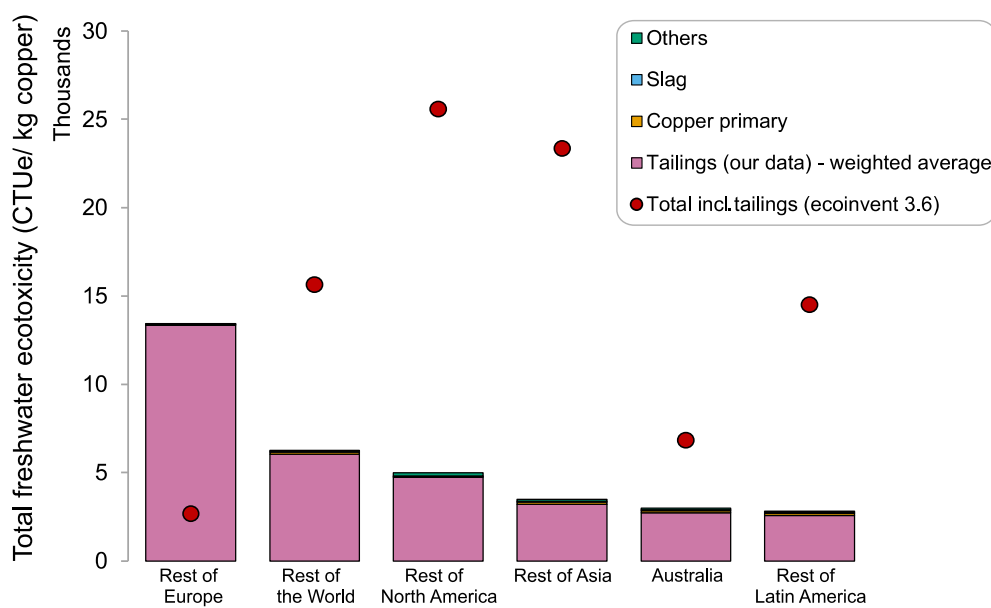


Figure S26. LCA of copper production (method: USEtox)—a) short-term and b) long-term in different regions. Data to generate this chart is available in Table S3.

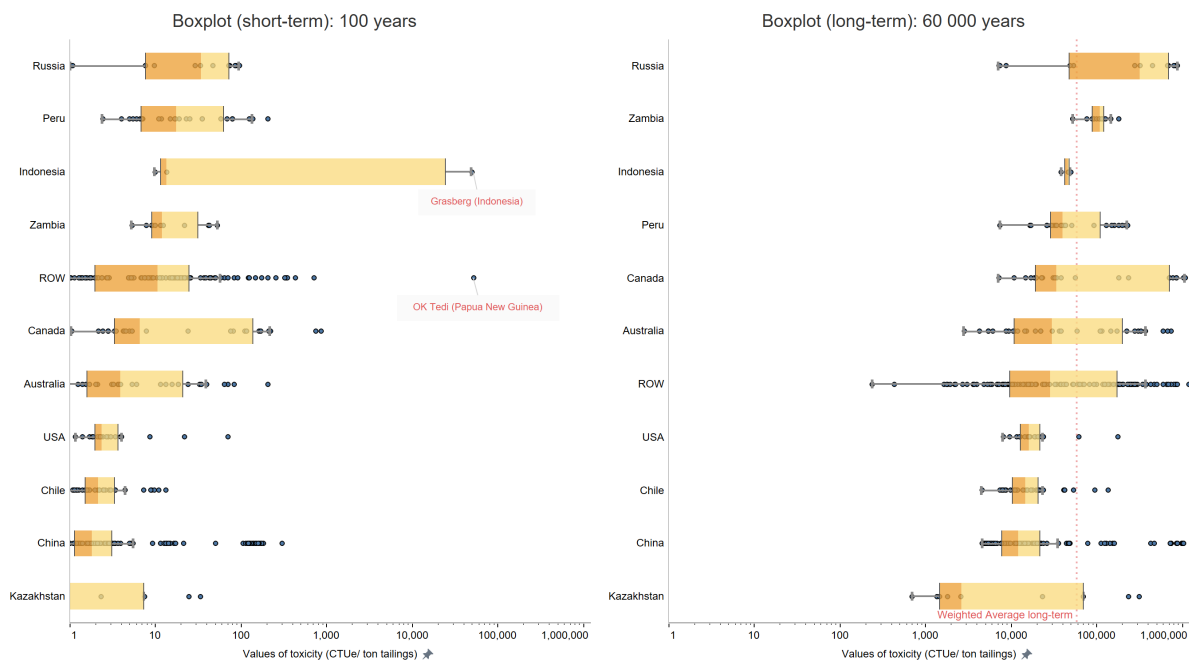
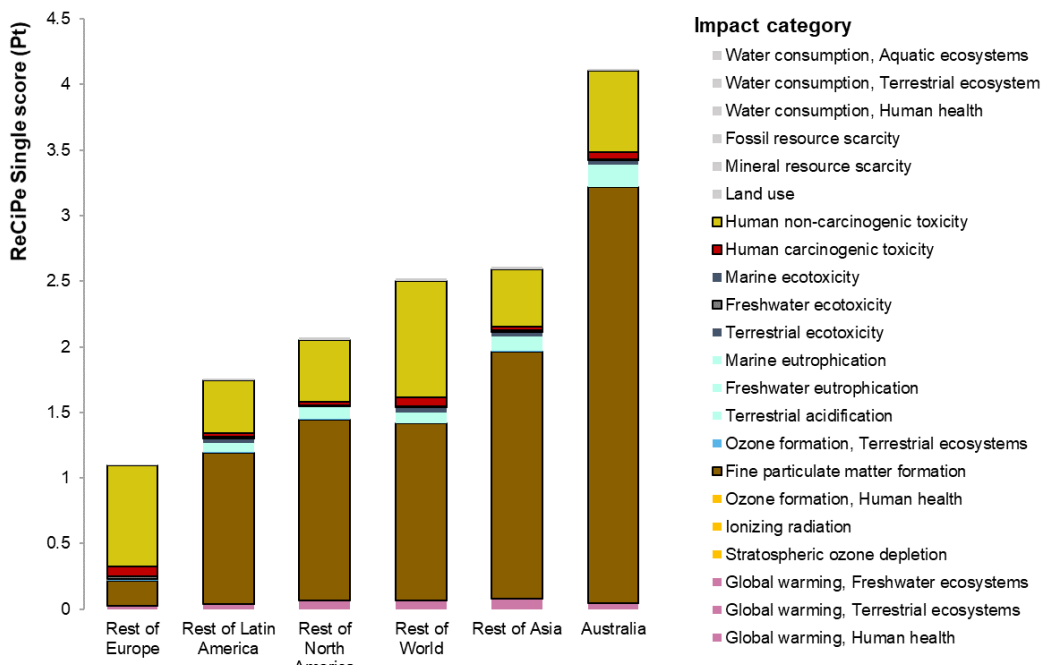


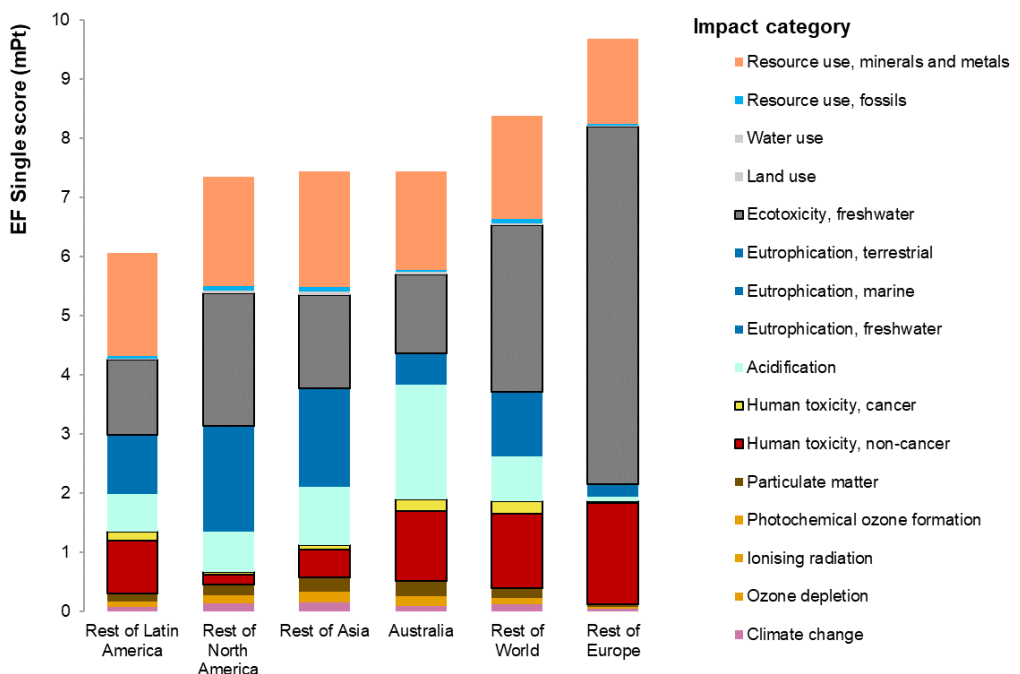
Figure S27. Freshwater ecotoxicity per ton of tailings in log-scale for short-term and long-term horizons

S15. Complementary LCA results: 1) USEtox human toxicity, midpoint, 2) ReCipe, endpoint single score, 3) EF 3.0, endpoint single score

The toxicity analyses in the main paper are based on the recommended UNEP-SETAC LCIA method, which is USEtox⁶⁵. The human toxicity results are documented in Supporting-Information 2, sheet 2.12 – 13. In general, the ecotoxicity and human toxicity assessments are almost the same, except that in the human-toxicity cancer category, Cu and Zn lack characterization factors. Furthermore, we also presented in Figure S28 the results for single score ReCipe endpoint methods and EF endpoint methods⁶⁶. This is to provide alternative views of the results in ranges of impact categories and to double check the consistencies across different methods. Compared to USEtox methods, which are behaving similarly between freshwater ecotoxicity and human toxicity, the results using ReCipe method are different. ReCipe shows that particulate matter formation and human toxicity as the major contributors in the whole system to produce 1 kg of copper. Furthermore, the weighting factors in ReCiPe are more spread to processes outside beneficiation systems (i.e., copper smelter and refinery), and therefore the emissions from these processes in the particulate matter formation category are high (in average 65% contribution to overall impacts across all continents due to sulfur dioxide and particulates). Single scores obtained from the EF methods, however, express the damages to wider categories like eutrophication and resource use, with ecotoxicity and human toxicity have 47% average contribution combined. Despite differences in the identification of priority life cycle stages of various LCIA methods, we can still conclude that metal leaching in the upstream stage is shown to be relevant for all methods (i.e., tailings long-term emission, demonstrated by Cu and Zn emissions in top process contributors in all continents as well as in the water compartment in S2.14). Other metal flows such as lead, arsenic, and cadmium are also present in the top flows that leach to the water compartment.



(A)



(B)

Figure S28. LCA results of 1 kg copper production. (A) ReCiPe single score, endpoint, incl. long-term emissions and (B) EF single score, endpoint, incl. long-term emissions)

S16. Further discussions and limitations on main waste streams in mining, rehabilitation, and tailings management

Besides discussions of data and limitations elaborated in the main manuscript, other aspects that require future improvements or care when interpreting the results are: (i) impacts from waste rock, overburden and other metallurgical slags/ residues, (ii) short term or continuous rehabilitation of tailings sites, and (iii) tailings disposal methods.

- (i) Other main waste streams such waste rock, overburden, slags, and other residues:** We need better and in-depth study to estimate the actual environmental impacts caused by its deposition. Acid mine drainage (AMD) could be a source of toxicity that can arise from the landfilling/ backfilling of overburdens. In our study, we applied cut-off to these wastes assuming its relatively benign characteristics with lower metal contents compared to tailings. Normally, the waste rock and overburden are mixed with cement paste for the making of backfill materials, rendering them stable. Thus, the ecotoxicity impacts from overburden/ waste rock are assumed to be negligible, as similarly implemented in the life cycle Ecoinvent database⁶⁷. We are aware of this limitation and thus recommend a better quantification and higher resolution of overburden/ waste rock impacts life cycle inventories in future research (besides limited coverage from reporting from companies⁶⁸). As for slags and other residues, Gordon (2002)⁶⁹ estimated the ratio of copper slags/ residues to metal in the US, which is equivalent to 2.1:1, compared to ~100:1 for tailings to metal ratio. To give an emphasis to the waste stream in this study and other important waste streams in the value chain, we present Figure S29.

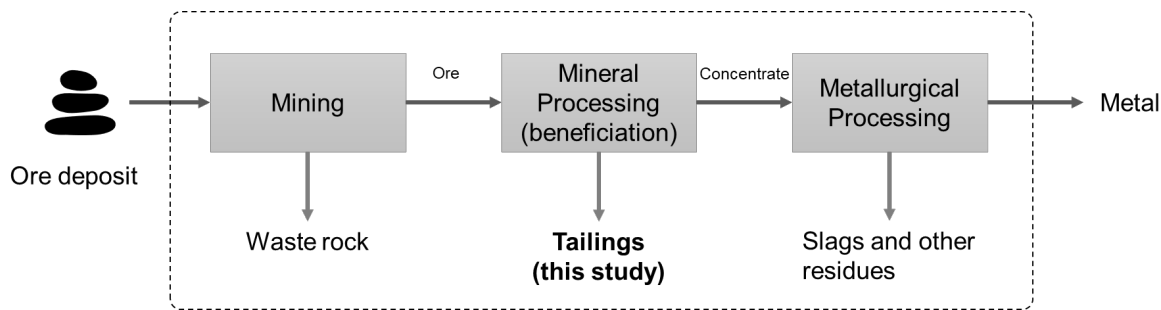


Figure S29. Simplified mining process flowsheets with the source of main waste flows (adapted from Lebre et al.⁷⁰)

- (ii) **Dust emissions:** Tailings are all assumed to enter soil and ultimately groundwater as the receiving compartment. In some cases, tailings can be carried away by wind and resulting in air/ dust emissions, sometimes the cases for the extremely arid regions. The environmental assessment studies for this case is somewhat limited; only one study tries to include the impacts through life cycle study from company reporting⁷¹. From their study, it is found that dust emissions would have in average 4% contribution to all toxicity indicators in short term assessment. While we did not include explicitly the modeling of dust in our study, future studies could investigate thoroughly the effects of local environments to understand the actual impacts of dust in the overall system.
- (iii) **Rehabilitation:** we assume estimate of leaching over long-term using cut-off temporal approach for disposal of waste, following what is done for other long-term waste disposals⁷². We use this as a default choice and aim to estimate the impacts of tailings on standard storage facility on land, except for notable sites where storage/ embankment structure is not feasible like in Indonesia and Papua New Guinea (more details for these sites or aqueous disposal is described below). In short term or during surveyable period, leaching of heavy metals does not influence the results and can be relatively ignored in the entire life cycle of metal production but the results would turn the complete opposite when long-term horizon is taken into account. We then suggest

further studies could expand the research in carrying out comparative analysis of different remediation or rehabilitation systems, either via active or passive mechanisms. This would also imply performing comparative analyses for continuous maintenance and operation for the duration of rehabilitation so that it can be used to select the optimized option and avoid burden shifting.

- (iv) **Tailings disposal and management.** There are various disposal methods for depositing tailings storage⁷³. Most of the cases, tailings are stored on land within dams with different types of structure. We choose this type of storage for all of the tailings landfill modeled in the present study, except for notable mines where direct disposals are practiced. Besides the standard impoundment behind a dam on land, common alternatives to conventional tailings dams are⁷⁴ (readers are invited to refer to the previous document for more information on tailings disposals):
- a. Backfilling: tailings are usually combined with binders like cement, then used to fill voids in underground operations. With this method, tailings are returned to their source. After a curing period, the backfill can act as the ground structure support and allow recovering ore from adjacent stope. Special type of backfills called cemented paste backfill—a mixture of tailings, water, and binder (e.g. Portland cement)—gained popularity owing to its mechanical strength and economics. However, as the volume of rock increases following milling, not all tailings can be returned to the pit or underground. There is still rooms for potentials for an improved backfill operation, for instances by using by-products from other industries such as fly ash and blast furnace slag as cement replacement⁷⁵.
 - b. Filtered tailings or sometimes called dry stack: tailings that have a reduced water content, or “filtered”, after mill processing. The resulting tailings are like a moist

soil and can be stacked in piles and compacted. However, filtered tailings can still lead to water contamination under certain circumstances.

- c. Aqueous dumping and submarine disposal: tailings are deposited directly into oceans, rivers, or streams. While there are many rationales such as unstable mountainous and extreme rainfalls for building proper storage facility⁷⁶, this direct disposal method is extremely destructive, polluting water, destroying ecosystems, and ruining livelihoods. Only a few jurisdictions⁷⁷ allow this choice of disposal due to extensive environmental loads to the environment. An analysis conducted by Earthworks in 2012 shows that million tons of mining waste are still discharged directly into rivers and seas, which prove to be irresponsible because of heavy metal contamination and milling chemicals. The extent of environmental impacts and its wide implications to the natural habitats and people's livelihood has been extensively discussed elsewhere^{78,79}.

S17. By-products and allocation in metal mining systems

The production of metals typically involves more than one product as the output. For instance, copper production is also linked with the other by-products such as zinc, gold, silver, cobalt, nickel, etc. In life cycle assessment (LCA), there are different ways to deal with multiple product systems: system expansion and allocation based on physical relationships or economic concepts⁸⁰. System expansion is seldom feasible for metal production because of the nonexistent single production or mono-output systems for the co-metals. Similarly, allocation due to physical relationships is not applicable in most cases. The alternative, suggested approaches are thus economic allocation or allocation based on physical properties (e.g. mass). On one hand, economic allocation suffers from the fact that metal prices may fluctuate over time, revealing dynamics that are not easily captured. The temporal scope chosen for prices can significantly affect the economic proportion and, therefore, the environmental impacts of metals and co-metals under study. On the other hand, physical allocation suffers from the fact that masses may be very disproportionate (e.g. very expensive low-concentration metals may be the reason for the mining activity, while less-valuable but higher concentration metals would be assigned the majority of the burdens). Thus, mass allocation does not reflect the economic reasons for doing the mining operation.

Studies such as those conducted by Memary et al. (2012)⁸¹, Nuss and Eckelman (2014)⁸², and Rötzer and Schmidt (2020)⁸³ show that more than 99% and 95% of impacts are allocated to copper, for mass and economic allocation respectively. Therefore, in this paper we simplified the analysis by allocating all impacts to copper. However, the data can be used to apply other allocation principles in future research. Overall, allocation choices and the effects of applying specific methods in the LCA of metals are still an open field that can benefit from more harmonization measures and in-depth future investigations^{84,85}.

In the case of deposits where geochemical zoning occurs, like VMS ore deposits, the processing configurations are set up to maximize the extraction of rich metals from the specific lithology. VMS deposits are compositionally zoned such that different areas or metal-laden zones are present with clear, distinctive characteristics⁸⁶: Cu- and Fe-rich sulfide being in the center and Zn- and Pb-rich sulfides concentrated at the outer margins (Figure S30).

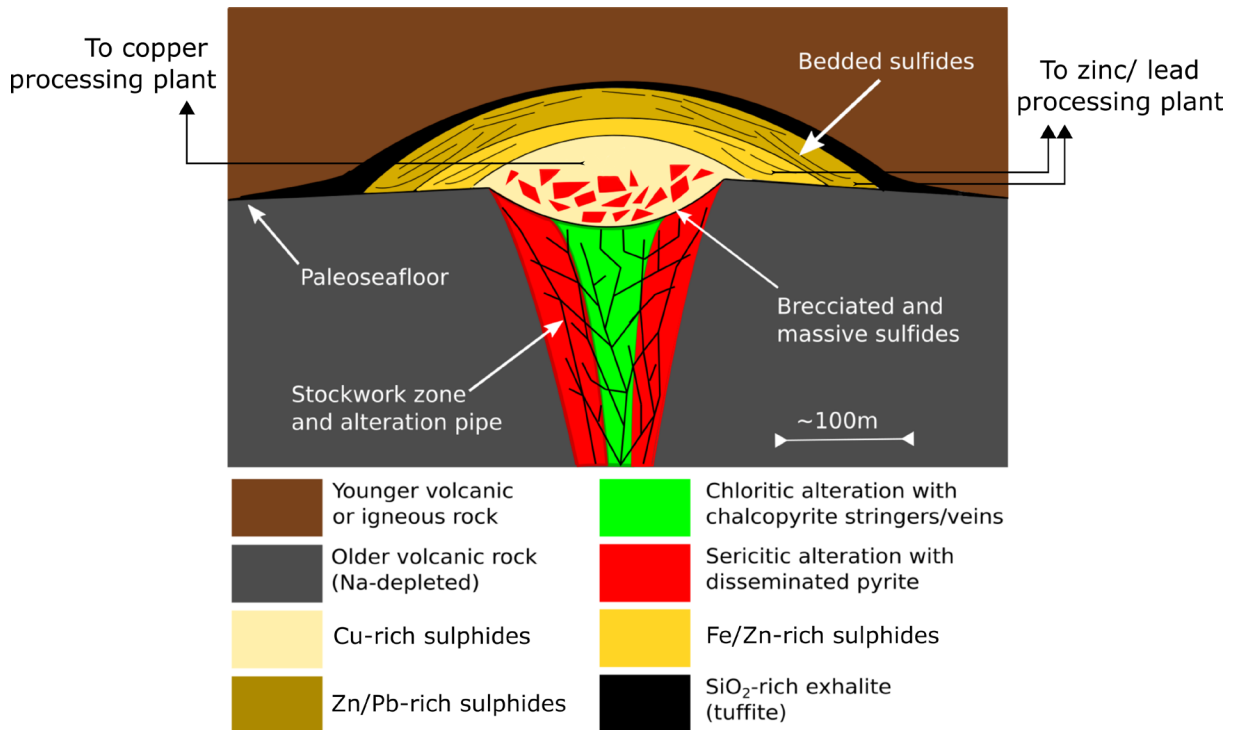


Figure S30. A cross-section of typical volcanogenic massive sulfide (VMS) as seen in the sedimentary record⁸⁶, image adapted from VMS webpage⁸⁷

Due to this geochemical zoning, VMS deposits were exploited at different treatment facilities, designed for extracting particular metal of interest, either copper or zinc/ lead. Taking the case of Iberian Pyrite Belt deposits, for instance, the mining and beneficiation of ore deposits comprise more than a single train to treat both copper-rich and zinc-rich mined materials. Copper deposits undergo mineral processing in the first unit that specifically extracts copper as the primary metal, while the second unit aims at primarily to treat zinc. Hence, these configurations already separate two metals (i.e., copper and zinc) in a different processing

plants where each has its own isolated systems. This suggests that environmental impacts of copper, in the first processing plant, has to be allocated with the emissions and energy/material consumption for this dedicated treatment plant only. This entire process is thus focused solely in producing concentrates with more than 96% copper volume in the same mine location; the rest is co-produced along with the zinc/ lead in the Zn-Pb processing plant. The common parts of the production system include the waste rock and tailings management.

S18. Further supporting information

There is a spreadsheet file that contains the data, specific resources, and assumptions for generating the results in this study. Individual values for each data point in the study are reported, either for the short-term or long-term horizons performed in LCA (S2.3). The LCIA results for human toxicity (USETox⁶⁵ method, carcinogenic and non-carcinogenic) are available in Supporting Information-2 (S2.12 – 13). We also performed LCA using ReCiPe⁸⁸ and EF as additional LCIA methods, which are tabulated in S2.14.

References

- (1) The R Core Team. R: The R Project for Statistical Computing <https://www.r-project.org/> (accessed Oct 22, 2020).
- (2) Wickham, H. *Ggplot2: Elegant Graphics for Data Analysis*; Use R!; Springer New York, 2009.
- (3) Tableau. Business Intelligence and Analytics Software <https://www.tableau.com/> (accessed Sep 25, 2020).
- (4) Microsoft. Spreadsheet Software Programs | Excel 365 <https://www.microsoft.com/en-us/microsoft-365/excel> (accessed Sep 25, 2020).
- (5) S&P. S&P Global Market Intelligence https://www.spglobal.com/marketintelligence/en/documents/112727-gics-mapbook_2018_v3_letter_digitalspreads.pdf (accessed Oct 10, 2019).
- (6) Mudd, G. M.; Weng, Z.; Jowitt, S. M. A Detailed Assessment of Global Cu Resource Trends and Endowments. *Econ. Geol.* **2013**, *108* (5), 1163–1183. <https://doi.org/10.2113/econgeo.108.5.1163>.
- (7) Norgate, T.; Jahanshahi, S. Low Grade Ores – Smelt, Leach or Concentrate? *Miner. Eng.* **2010**, *23* (2), 65–73. <https://doi.org/10.1016/J.MINENG.2009.10.002>.
- (8) Ayres, R. U.; Ayres, L. W.; Råde, I. *The Life Cycle of Copper, Its Co-Products and By-Products (Report for Mining, Minerals and Sustainable Development, No. 24)*; 2002.
- (9) Metso Outotec. HSC Chemistry <https://www.outotec.com/products-and-services/technologies/digital-solutions/hsc-chemistry/> (accessed Jun 5, 2020).
- (10) Michaux, B.; Hannula, J.; Rudolph, M.; Reuter, M. A.; van den Boogaart, K. G.; Möckel, R.; Kobylin, P.; Hultgren, M.; Peltomäki, M.; Roine, A.; Remes, A. Water-Saving Strategies in the Mining Industry – The Potential of Mineral Processing Simulators as a Tool for Their Implementation. *J. Environ. Manage.* **2019**, *234*, 546–553. <https://doi.org/10.1016/j.jenvman.2018.11.139>.
- (11) Ferreira, J. P.; Loveday, B. K. Improved Model for Simulation of Flotation Circuits. *Miner. Eng.* **2000**, *13* (14–15), 1441–1453. [https://doi.org/10.1016/S0892-6875\(00\)00129-1](https://doi.org/10.1016/S0892-6875(00)00129-1).
- (12) Bulatovic, S. M. *Handbook of Flotation Reagents: Chemistry, Theory and Practice Flotation of Sulfide Ores*; Elsevier, 2007. <https://doi.org/10.1016/B978-0-444-53029-5.X5009-6>.
- (13) Wills, B. A.; Finch, J. A. Froth Flotation. In *Wills' Mineral Processing Technology*; Wills, B. A., Finch, J. A., Eds.; Butterworth-Heinemann: Boston, 2016; pp 265–380. <https://doi.org/10.1016/b978-0-08-097053-0.00012-1>.
- (14) King, R. P. Flotation. In *Modeling and Simulation of Mineral Processing Systems*; Elsevier, 2001; pp 289–350. <https://doi.org/10.1016/B978-0-08-051184-9.50013-4>.
- (15) Seal, R. R.; Nadine, M. Environmental Attributes and Resource Potential of Mill Tailings from Diverse Mineral Deposit Types. In *Mine Water and Circular Economy*; Lappeenranta, 2017.
- (16) Bakalarz, A. Chemical and Mineral Analysis of Flotation Tailings from Stratiform Copper Ore from Lubin Concentrator Plant (SW Poland). *Mineral Processing and Extractive Metallurgy Review*. Taylor and Francis Inc. November 2, 2019, pp 437–446. <https://doi.org/10.1080/08827508.2019.1667778>.
- (17) Martín-Crespo, T.; Gómez-Ortiz, D.; Martín-Velázquez, S. Geoenvironmental Characterization of Sulfide Mine Tailings. In *Applied Geochemistry with Case Studies on Geological Formations, Exploration Techniques and Environmental Issues*;

- IntechOpen, 2020. <https://doi.org/10.5772/intechopen.84795>.
- (18) Nadeif, A.; Taha, Y.; Bouzahzah, H.; Hakkou, R.; Benzaazoua, M. Desulfurization of the Old Tailings at the Au-Ag-Cu Tiouit Mine (Anti-Atlas Morocco). *Minerals* **2019**, *9* (7), 401. <https://doi.org/10.3390/min9070401>.
- (19) Hällström, L. P. B.; Alakangas, L.; Martinsson, O. Geochemical Characterization of W, Cu and F Skarn Tailings at Yxsjöberg, Sweden. *J. Geochemical Explor.* **2018**, *194*, 266–279. <https://doi.org/10.1016/J.GEXPLO.2018.09.001>.
- (20) Misra, K. C. Skarn Deposits BT - Understanding Mineral Deposits; Misra, K. C., Ed.; Springer Netherlands: Dordrecht, 2000; pp 414–449. https://doi.org/10.1007/978-94-011-3925-0_9.
- (21) Craw, D.; Cavanagh, J.; Druzbicka, J.; Harding, J. S.; Kerr, G.; Pope, J.; Trumm, D. A Geoenvironmental Model for Orogenic Gold Deposits to Predict Potential Environmental Effects. *Mine Water Environ.* **2015**, *34* (4), 388–403. <https://doi.org/10.1007/s10230-015-0358-0>.
- (22) Schulz, K. J.; Chandler, V. W.; Nicholson, S. W.; Piatak, N.; Seal, R. R.; Woodruff, L. G.; Zientek, M. L. *Magmatic Sulfide-Rich Nickel-Copper Deposits Related to Picrite and (or) Tholeiitic Basalt Dike-Sill Complexes: A Preliminary Deposit Model*.
- (23) Placencia-Gómez, E.; Parviainen, A.; Hokkanen, T.; Loukola-Ruskeeniemi, K. Integrated Geophysical and Geochemical Study on AMD Generation at the Haveri Au-Cu Mine Tailings, SW Finland. *Environ. Earth Sci.* **2010**, *61* (7), 1435–1447. <https://doi.org/10.1007/s12665-010-0459-9>.
- (24) Triantafyllidis, S.; Skarpelis, N.; Komnitsas, K. Environmental Characterization and Geochemistry of Kirki, Thrace, NE Greece, Abandoned Flotation Tailing Dumps. *Environ. Forensics* **2007**, *8* (4), 351–359. <https://doi.org/10.1080/15275920701729688>.
- (25) Forsythe, N. A.; Spry, P. G.; Thompson, M. L. Petrological and Mineralogical Aspects of Epithermal Low-Sulfidation Au-and Porphyry Cu-Style Mineralization, Navilawa Caldera, Fiji. *Geosci.* **2019**, *9* (1), 42. <https://doi.org/10.3390/geosciences9010042>.
- (26) Velásquez, G.; Carrizo, D.; Salvi, S.; Vela; Pablo; Pérez. Tracking Cobalt, REE and Gold from a Porphyry-Type Deposit by LA-ICP-MS: A Geological Approach towards Metal-Selective Mining in Tailings. *Minerals* **2020**, *10*, 109. <https://doi.org/10.3390/min10020109>.
- (27) Heinrich, C. A.; Candela, P. A. Fluids and Ore Formation in the Earth's Crust. In *Treatise on Geochemistry: Second Edition*; Elsevier Inc., 2013; Vol. 13, pp 1–28. <https://doi.org/10.1016/B978-0-08-095975-7.01101-3>.
- (28) Berger, B. R.; Ayuso, R. A.; Wynn, J. C.; Seal, R. R. *Preliminary Model of Porphyry Copper Deposits Open-File Report 2008-1321*.
- (29) Parkhurst, D.; Appelo, T. *Parkhurst DL, Appelo CAJ (2013) Description of Input and Examples for PHREEQC Version 3—a Computer Program for Speciation, Batch-Reaction, One-Dimensional Transport, and Inverse Geochemical Calculations. US Geological Survey Techniques and Methods, Book 6*; 2013.
- (30) Ball, J. W.; Nordstrom, D. K. *User's Manual for WATEQ4F, with Revised Thermodynamic Data Base and Text Cases for Calculating Speciation of Major, Trace, and Redox Elements in Natural Waters, Version 2.*; 1991. <https://doi.org/10.3133/ofr91183>.
- (31) Hyks, J.; Astrup, T.; Christensen, T. H. Long-Term Leaching from MSWI Air-Pollution-Control Residues: Leaching Characterization and Modeling. *J. Hazard. Mater.* **2009**, *162* (1), 80–91. <https://doi.org/10.1016/J.JHAZMAT.2008.05.011>.
- (32) Hyks, J. Leaching from Municipal Solid Waste Incineration Residues, DTU Denmark, 2008.
- (33) Tiruta-Barna, L. Using PHREEQC for Modelling and Simulation of Dynamic Leaching Tests and Scenarios. *J. Hazard. Mater.* **2008**, *157* (2–3), 525–533.

- https://doi.org/10.1016/j.jhazmat.2008.01.028.
- (34) Sieland, R.; Metschies, T.; Jahn, S. Reactive Transport Modelling of the Contaminant Release from Uranium Tailings Using PhreeqC / Excel-Coupling. *Min. Meets Water – Conflicts Solut.* **2016**, 1234–1241.
- (35) Dzombak, D. A.; Morel, F. M. M. *Surface Complexation Modeling: Hydrous Ferric Oxide*; John Wiley & Sons, 1990.
- (36) Appelo, C. A. J.; Van Der Weiden, M. J. J.; Tournassat, C.; Charlet, L. Surface Complexation of Ferrous Iron and Carbonate on Ferrihydrite and the Mobilization of Arsenic. *Environ. Sci. Technol.* **2002**, 36 (14), 3096–3103.
https://doi.org/10.1021/es010130n.
- (37) Parkhurst, D. L.; Appelo, C. A. J.; Survey, U. S. G. *Description of Input and Examples for PHREEQC Version 3: A Computer Program for Speciation, Batch-Reaction, One-Dimensional Transport, and Inverse Geochemical Calculations*; Reston, VA, 2013.
https://doi.org/10.3133/tm6A43.
- (38) Rowe, R. K.; Islam, M. Z. Impact of Landfill Liner Time-Temperature History on the Service Life of HDPE Geomembranes. *Waste Manag.* **2009**, 29 (10), 2689–2699.
https://doi.org/10.1016/j.wasman.2009.05.010.
- (39) Gorakhki, M. H.; Bareither, C. A. Sustainable Reuse of Mine Tailings and Waste Rock as Water-Balance Covers. *Minerals* **2017**, 7 (7), 128.
https://doi.org/10.3390/min7070128.
- (40) Shamsai, A.; Pak, A.; Bateni, S. M.; Ayatollahi, S. A. H. Geotechnical Characteristics of Copper Mine Tailings: A Case Study. *Geotech. Geol. Eng.* **2007**, 25 (5), 591–602.
https://doi.org/10.1007/s10706-007-9132-9.
- (41) Gitari, W. M.; Thobakgale, R.; Akinyemi, S. A. Mobility and Attenuation Dynamics of Potentially Toxic Chemical Species at an Abandoned Copper Mine Tailings Dump. *Minerals* **2018**, 8 (2), 64. https://doi.org/10.3390/min8020064.
- (42) Mahmood, A. A.; Elektorowicz, M. An Investigation of the Porosity Dependent Strength and Leachability of Mine Tailings Matrices Containing Heavy Metals. *Cogent Environ. Sci.* **2020**, 6 (1). https://doi.org/10.1080/23311843.2020.1743626.
- (43) Porter, K. E.; Bleiwas, D. I. *Physical Aspects of Waste Storage from a Hypothetical Open Pit Porphyry Copper Operation*, Version 1.; 2003.
https://doi.org/10.3133/ofr03143.
- (44) Lyu, Z.; Chai, J.; Xu, Z.; Qin, Y.; Cao, J. A Comprehensive Review on Reasons for Tailings Dam Failures Based on Case History. *Adv. Civ. Eng.* **2019**, 2019, 4159306.
https://doi.org/10.1155/2019/4159306.
- (45) SULTAN. *Tailings Data and Properties from Partnering Companies (Internal Exchanges)*; Leuven, 2019.
- (46) Hu, L.; Wu, H.; Zhang, L.; Zhang, P.; Wen, Q. Geotechnical Properties of Mine Tailings. *J. Mater. Civ. Eng.* **2017**, 29 (2), 04016220.
https://doi.org/10.1061/(ASCE)MT.1943-5533.0001736.
- (47) European Commission. ANNEX 3 to the Commission Staff Working Document Accompanying the Report from the Commission in Accordance with Article 3.7 of the Groundwater Directive 2006/118/EC on the Establishment of Groundwater Threshold Values Information on the Groundwater Thresh. **2009**, No. January 2009, 1–76.
https://doi.org/10.1017/CBO9781107415324.004.
- (48) Sutanudjaja, E. H.; van Beek, R.; Wanders, N.; Wada, Y.; Bosmans, J. H. C.; Drost, N.; van der Ent, R. J.; de Graaf, I. E. M.; Hoch, J. M.; de Jong, K.; Karssenberg, D.; López López, P.; Peßenteiner, S.; Schmitz, O.; Straatsma, M. W.; Vannametee, E.; Wisser, D.; Bierkens, M. F. P. PCR-GLOBWB 2: A 5 Arcmin Global Hydrological and Water Resources Model. *Geosci. Model Dev.* **2018**, 11 (6), 2429–2453.
https://doi.org/10.5194/gmd-11-2429-2018.

- (49) Wada, Y.; Van Beek, L. P. H.; Van Kempen, C. M.; Reckman, J. W. T. M.; Vasak, S.; Bierkens, M. F. P. Global Depletion of Groundwater Resources. *Geophys. Res. Lett.* **2010**, *37* (20). <https://doi.org/10.1029/2010GL044571>.
- (50) Elshkaki, A.; Graedel, T. E.; Ciacci, L.; Reck, B. Copper Demand, Supply, and Associated Energy Use to 2050. *Glob. Environ. Chang.* **2016**, *39*, 305–315. <https://doi.org/10.1016/j.gloenvcha.2016.06.006>.
- (51) Elshkaki, A.; Graedel, T. E.; Ciacci, L.; Reck, B. K. Resource Demand Scenarios for the Major Metals. *Environ. Sci. Technol.* **2018**, *52* (5), 2491–2497. <https://doi.org/10.1021/acs.est.7b05154>.
- (52) Northey, S.; Mohr, S.; Mudd, G. M.; Weng, Z.; Giurco, D. Modelling Future Copper Ore Grade Decline Based on a Detailed Assessment of Copper Resources and Mining. *Resour. Conserv. Recycl.* **2014**, *83*, 190–201. <https://doi.org/10.1016/j.resconrec.2013.10.005>.
- (53) ICMM. Understanding Risks and Lessons from Sustainability : ICMM and Its Role. **2015**, No. January.
- (54) SERNAGEOMIN. *Geochemistry of Surface Samples of the Tailings Deposits in Chile*; 2020.
- (55) Hervé, M.; Sillitoe, R. H.; Wong, C.; Fernández, P.; Crignola, F.; Ipinza, M.; Urzúa, F. Geologic Overview of the Escondida Porphyry Copper District, Northern Chile. In *Geology and Genesis of Major Copper Deposits and Districts of the World: A Tribute to Richard H. Sillitoe*; 2020; Vol. 16, pp 55–78. <https://doi.org/10.5382/sp.16.03>.
- (56) Padilla Garza, R. A.; Titley, S. R.; Pimentel B, F. Geology of the Escondida Porphyry Copper Deposit, Antofagasta Region, Chile. *Econ. Geol.* **2001**, *96* (2), 307–324. <https://doi.org/10.2113/gsecongeo.96.2.307>.
- (57) Guang-Yi, L.; Hong, Z.; Liu-Yin, X.; Shuai, W.; Zheng-He, X. Improving Copper Flotation Recovery from a Refractory Copper Porphyry Ore by Using Ethoxycarbonyl Thiourea as a Collector. *Miner. Eng.* **2011**, *24* (8), 817–824. <https://doi.org/10.1016/j.mineng.2011.01.009>.
- (58) Asghari, M.; Nakhaei, F.; VandGhorbany, O. Copper Recovery Improvement in an Industrial Flotation Circuit: A Case Study of Sarcheshmeh Copper Mine. *41* (6), 761–778. <https://doi.org/10.1080/15567036.2018.1520356>.
- (59) Alcalde, J.; Kelm, U.; Vergara, D. Historical Assessment of Metal Recovery Potential from Old Mine Tailings: A Study Case for Porphyry Copper Tailings, Chile. *Miner. Eng.* **2018**, *127*, 334–338. <https://doi.org/10.1016/j.mineng.2018.04.022>.
- (60) Lynch, A. J. *Mineral and Coal Flotation Circuits: Their Simulation and Control*; Developments in mineral processing; Elsevier Scientific Publishing Company, 1981.
- (61) Pease, J. D.; Curry, D. C.; Young, M. F. Designing Flotation Circuits for High Fines Recovery. In *Minerals Engineering*; Pergamon, 2006; Vol. 19, pp 831–840. <https://doi.org/10.1016/j.mineng.2005.09.056>.
- (62) Kohmuench, J. N.; Mankosa, M. J.; Thanasekaran, H.; Hobert, A. Improving Coarse Particle Flotation Using the HydroFloat™ (Raising the Trunk of the Elephant Curve). *Miner. Eng.* **2018**, *121*, 137–145. <https://doi.org/10.1016/j.mineng.2018.03.004>.
- (63) USGS. Mineral Resources Online Spatial Data: Interactive maps and downloadable data for regional and global analysis <https://mrdata.usgs.gov/#mineral-resources>.
- (64) Mudd, G. M.; Jowitt, S. M. Growing Global Copper Resources, Reserves and Production: Discovery Is Not the Only Control on Supply. *Econ. Geol.* **2018**, *113* (6), 1235–1267. <https://doi.org/10.5382/econgeo.2018.4590>.
- (65) Rosenbaum, R. K.; Bachmann, T. M.; Gold, L. S.; Huijbregts, M. A. J.; Jolliet, O.; Jurasko, R.; Koehler, A.; Larsen, H. F.; MacLeod, M.; Margni, M.; McKone, T. E.; Payet, J.; Schuhmacher, M.; van de Meent, D.; Hauschild, M. Z. USEtox—the UNEP-SETAC Toxicity Model: Recommended Characterisation Factors for Human Toxicity

- and Freshwater Ecotoxicity in Life Cycle Impact Assessment. *Int. J. Life Cycle Assess.* **2008**, *13* (7), 532. <https://doi.org/10.1007/s11367-008-0038-4>.
- (66) Fazio, S.; Castellani, V.; Sala, S.; Erwin, S.; Secchi, M.; Zampori, L.; Diaconu, E. *Supporting Information to the Characterisation Factors of Recommended EF Life Cycle Impact Assessment Method*; Ispra: European Commission, 2018. <https://doi.org/10.2760/671368>.
- (67) Classen, M.; Althaus, H.-J.; Blaser, S.; Tuchschnid, M.; Jungbluth, N.; Doka, G.; Emmenegger, M. F.; Schärnhorst, W. Life Cycle Inventories of Metals. Final Report Ecoinvent Data v2.1, No 10. *Ecoinvent* **2009**, No. 10.
- (68) Mudd, G. Waste Not Want Not - Queensland Mining & Energy Bulletin <https://www.qmemb.com.au/waste-want/> (accessed Nov 1, 2021).
- (69) Gordon, R. B. Production Residues in Copper Technological Cycles. *Resour. Conserv. Recycl.* **2002**, *36* (2), 87–106. [https://doi.org/10.1016/S0921-3449\(02\)00019-8](https://doi.org/10.1016/S0921-3449(02)00019-8).
- (70) Lèbre, É.; Corder, G.; Golev, A. The Role of the Mining Industry in a Circular Economy: A Framework for Resource Management at the Mine Site Level. *J. Ind. Ecol.* **2017**, *21* (3), 662–672. <https://doi.org/10.1111/jiec.12596>.
- (71) Beylot, A.; Villeneuve, J. Accounting for the Environmental Impacts of Sulfidic Tailings Storage in the Life Cycle Assessment of Copper Production: A Case Study. *J. Clean. Prod.* **2017**, *153*, 139–145. <https://doi.org/10.1016/j.jclepro.2017.03.129>.
- (72) Doka, G.; Hischier, R. Waste Treatment and Assessment of Long-Term Emissions. *International Journal of Life Cycle Assessment*. Springer December 6, 2005, pp 77–84. <https://doi.org/10.1065/lca2004.12.181.9>.
- (73) Ellis, D. *Environmental Impact Assessment Guidelines for Mine Development and Tailings Disposal at Tropical Coastal Mines*; 1996.
- (74) Wills, B. A.; Finch, J. A. Tailings Disposal. In *Wills' Mineral Processing Technology*; Butterworth-Heinemann, 2016; pp 439–448. <https://doi.org/10.1016/b978-0-08-097053-0.00016-9>.
- (75) Peyronnard, O.; Benzaazoua, M. Estimation of the Cementitious Properties of Various Industrial By-Products for Applications Requiring Low Mechanical Strength. *Resour. Conserv. Recycl.* **2011**, *56* (1), 22–33. <https://doi.org/10.1016/j.resconrec.2011.08.008>.
- (76) Vogt, C. International Assessment of Marine and Riverine Disposal of Mine Tailings: Final Report Adopted by the International Maritime Organization, London Convention/Protocol http://www.craigvogt.com/links/Mine_Tailings_Marine_and_Riverine_Disposal.pdf (accessed Jun 30, 2021).
- (77) Vogt, C. International Assessment of Marine and Riverine Disposal of Mine Tailings. In *Impact Assessment for Social and Economic Development - 34th Annual Conference of the International Association for I*; 2012; pp 1–134.
- (78) Mckinnon, E. The Environmental Effects of Mining Waste Disposal at Lihir Gold Mine , Papua New Guinea. *J. Rural Remote Environ. Heal.* **2002**, *1* (2), 40–50.
- (79) Vare, L. L.; Baker, M. C.; Howe, J. A.; Levin, L. A.; Neira, C.; Ramirez-Llodra, E. Z.; Reichelt-Brushett, A.; Rowden, A. A.; Shimmield, T. M.; Simpson, S. L.; Soto, E. H. Scientific Considerations for the Assessment and Management of Mine Tailings Disposal in the Deep Sea. *Frontiers in Marine Science*. Frontiers February 5, 2018, p 17. <https://doi.org/10.3389/fmars.2018.00017>.
- (80) Santero, N.; Hendry, J. Harmonization of LCA Methodologies for the Metal and Mining Industry. *Int. J. Life Cycle Assess.* **2016**, *21* (11), 1543–1553. <https://doi.org/10.1007/s11367-015-1022-4>.
- (81) Memary, R.; Giurco, D.; Mudd, G.; Mason, L. Life Cycle Assessment: A Time-Series Analysis of Copper. *J. Clean. Prod.* **2012**, *33*, 97–108. <https://doi.org/10.1016/j.jclepro.2012.04.025>.

- (82) Nuss, P.; Eckelman, M. J. Life Cycle Assessment of Metals: A Scientific Synthesis. *PLoS One* **2014**, 9 (7), e101298. <https://doi.org/10.1371/journal.pone.0101298>.
- (83) Rötzer, N.; Schmidt, M. Historical, Current, and Future Energy Demand from Global Copper Production and Its Impact on Climate Change. *Resources* **2020**, 9 (4), 44. <https://doi.org/10.3390/RESOURCES9040044>.
- (84) Weidema, B. Avoiding Co-Product Allocation in Life-Cycle Assessment. *J. Ind. Ecol.* **2000**, 4 (3), 11–33. <https://doi.org/10.1162/108819800300106366>.
- (85) Weidema, B. P.; Schmidt, J. H. Avoiding Allocation in Life Cycle Assessment Revisited. *Journal of Industrial Ecology*. March 2010, pp 192–195. <https://doi.org/10.1111/j.1530-9290.2010.00236.x>.
- (86) Hannington, M. D. Volcanogenic Massive Sulfide Deposits. In *Treatise on Geochemistry: Second Edition*; Elsevier, 2013; Vol. 13, pp 463–488. <https://doi.org/10.1016/B978-0-08-095975-7.01120-7>.
- (87) Wikipedia. Volcanogenic massive sulfide ore deposit - Wikipedia https://www.wikiwand.com/en/Volcanogenic_massive_sulfide_ore_deposit (accessed Nov 4, 2021).
- (88) Huijbregts, M. A. J. J.; Steinmann, Z. J. N. N.; Elshout, P. M. F. F.; Stam, G.; Verones, F.; Vieira, M.; Zijp, M.; Hollander, A.; van Zelm, R. ReCiPe2016: A Harmonised Life Cycle Impact Assessment Method at Midpoint and Endpoint Level. *Int. J. Life Cycle Assess.* **2017**, 22 (2), 138–147. <https://doi.org/10.1007/s11367-016-1246-y>.